Probability distributions of continuous measurement results for two noncommuting variables and postselected quantum evolution

A. Franquet* and Yuli V. Nazarov
Kavli Institute of Nanoscience, Delft University of Technology, 2628 CJ Delft, The Netherlands

(Received 22 June 2019; published 6 December 2019)

We address the statistics of a simultaneous continuous weak linear measurement of two noncommuting variables on a few-state quantum system subject to a postselected evolution. The results of both postselected quantum measurement and simultaneous monitoring of two noncommuting variables differ drastically from the results of either classical or quantum projective measurement. We explore the peculiarities arising from the combination of the two. We concentrate on the distribution function of two measurement outcomes integrated over a time interval. We formulate a proper formalism for the evaluation of such distribution, and further compute and discuss the resulting statistics for idealized and experimentally relevant setups. We demonstrate the visibility and manifestations of the interference between initial and final states in the statistics of measurement outcomes for both variables in various regimes. We analytically predict the peculiarities at the circle $\mathcal{O}_1^2 + \mathcal{O}_2^2 = 1$ in the distribution of measurement outcomes $\mathcal{O}_{1,2}$ in the limit of short measurement times and confirm this by numerical calculation at longer measurement times. We demonstrate analytically the anomalously large values of the time-integrated output cumulants in the limit of short measurement times and zero overlap between initial and final states, and give the detailed distributions for this case. We term this situation *sudden jump*. We present the numerical evaluation of the probability distributions for experimentally relevant parameters in several regimes and demonstrate that interference effects in the postselected measurement can be accurately predicted even if they are small.

DOI: 10.1103/PhysRevA.100.062109

I. INTRODUCTION

Quantum computing and communication [1] are stimulating a rapid progress in the understanding and control of small quantum systems. An important ingredient for advanced quantum control is the ability to realize continuous monitoring, or measurement, of a quantum system. Theories of continuous quantum measurement [2–8] and experiments [9–15] have enabled a detailed understanding of the realisitic and practical measurement processes on quantum few-state systems.

An interesting and relevant case of quantum measurement is the measurement of noncommuting quantum variables. The fact that some observables *cannot* be measured together is one of the major differences between quantum and classical theory. The simultaneous measurement of noncommuting variables for a long time has been a topic of many experimental and theoretical studies in quantum optics [16]. The linearity of most optical measurements provides a perfect platform for experiments of this kind. However, only recently [4,6,17–20] the simultaneous monitoring of noncommuting variables has been studied in the context of the qubits.

Another interesting and relevant kind of quantum measurement is the postselected measurement. It implies postselection of the detector results accumulated on a time interval on the result of the projective measurement. The statistics of detector readings is thus accumulated only if the system ends up in a certain fixed state. Thus, for a general postselected evolution, both the initial and final states of the system can be regarded as fixed. It has been shown that the statistics of such a postselected measurement may drastically differ from the unselected case [5,6]. In this context, the statistics of measurement results reveal distinctly quantum phenomena that can be interpreted in terms of weak values [21] and are associated with the interference of initial and final states [22,23].

This paper elaborates on a combined case of quantum measurement of two noncommuting variables and for postselected quantum evolution. The goal is to evaluate the full statistics of the measurement results and its dependence on the dynamics of the system measured. For that purpose, we use the theory of continuous weak linear measurements, where a sufficiently weak coupling between a quantum system and infinitely many degrees of freedom of a linear detector provides their entanglement and conversion of the (discrete) quantum information into continuous time-dependent readings of the detector [2–8]. Our particular approach to continuous weak linear measurement statistics was first introduced in [6,24], and has been extended to include postselected evolution in [25]. It is based on the theory of full counting statistics in the extended Keldysh formalism [26]. The statistics of measurements of $\int dt\, \hat{V}(t)$, $V(t)$ being a quantum mechanical variable representing linear degrees of freedom that are measured, are evaluated with the characteristic functional method and the use of counting-field technique. The method provides the necessary and compact

*A.FranquetGonzalez@tudelft.nl

description of the whole quantum system consisting of the measured system and multiple degrees of freedom describing general linear detectors.

The probability distributions for the measurement of a single variable have been extensively studied in our recent publication [25]. The motivation to address the two-variable case comes from the recent experiments [12] where a qubit has been measured in a resonance fluorescence setup. In the experiment, the transmon qubit enclosed in a nonresonant three-dimensional (3D) superconducting cavity is resonantly driven at the Rabi frequency Ω and its fluorescence signal is recorded. The cavity is coupled to two transmission lines, the resonant driving field drives the qubit via a weakly coupled line, while most of the fluorescence signal exits via the other line which is coupled strongly. The complex amplitude of the the fluorescence signal is proportional to σ_-, the average of the lowering operator $\hat{\sigma}_- = |g\rangle\langle e|$ of the qubit, and oscillates with the Rabi frequency Ω. At each run, the qubit is prepared in either its ground $|g\rangle$ or excited $|e\rangle$ state and the signal is monitored during a time interval $(0, \mathcal{T})$. At time $\mathcal{T}$, the qubit is projectively measured using a strong pulse at the bare cavity frequency.

A heterodyne detection setup is used to measure this signal, and the fluorescence signal can be interpreted as a result of a weak continuous measurement. We notice that the experiment discussed can give access not only to the postselected averages, but also to the postselected statistics of the measurement results. Those are statistics of the continuous weak measurement of two noncommuting variables of the qubit, σ_x and σ_y, that comprise $\hat{\sigma}_- = \hat{\sigma}_x - i\hat{\sigma}_y$.

The statistics of the postselected measurement results reveal the signatures of interference between preselected and postselected states. With this work, we extend these signatures to the case of simultaneous measurement of noncommuting variables, and study the visibility of these signatures in dependence on the qubit dynamics in different parameter regimes.

Our results demonstrate that one can achieve very detailed theoretical predictions of the statistics of continuous weak linear measurement of two noncommuting variables, with account for every relevant experimental parameter. This allows for the study and characterization of quantum effects at any choice of parameters, even in the regime where the signatures are very weak.

Let us shortly highlight important and interesting results obtained in this article.

We show that the joint distribution of measurement outcomes of two noncommuting quantum variables $P(\mathcal{O}_1, \mathcal{O}_2)$ has peculiarities located at the circle $\mathcal{O}_1^2 + \mathcal{O}_2^2 = 1$ if $\mathcal{O}_{1,2}$ correspond to $\sigma_{x,y}$. This is the two-variable analog of the *half-quantized* measurement values for the single-variable measurement case. We reveal these peculiarities by analytical calculation of the quasidistribution of shifts of the normal distributions in the limit of short measurement time, and demonstrate them in numerical results at larger measurement times. We investigate how the visibility of the circle is suppressed by the system dynamics, such that the joint distribution in the limit of large suppression becomes a product of two independent distributions $P(\mathcal{O}_1, \mathcal{O}_2) \approx P_1(\mathcal{O}_1)P_2(\mathcal{O}_2)$.

At measurement times that are so short that the wave function of the system does not change significantly, and in the case of zero or small overlap between initial and final states, we reveal anomalously large values of the cumulants of the distribution function of time-integrated outputs. As we explain in [25] where this phenomenon has been considered in the single-variable case, such strong increase of the cumulants at a short time interval is worth nicknaming a *sudden jump*. Although it sounds like a slang, we will use it throughout the paper an as abbreviation. For the average value of the output, that is the first cumulant, its big value is readily understood from the weak value theory [21]. In the case of simultaneous measurement of two noncommuting variables, we reveal simultaneous *sudden jump* of the two time-integrated outputs $\mathcal{O}_1, \mathcal{O}_2$ with an appropriate choice of the qubit Hamiltonian. We present both analytical and numerical results. We also compute the distributions of the outputs under realistic experimental parameters of [12] concentrating on the quantum signatures of postselected evolution and the noncommutativity of the variables.

Let us explain the structure of the paper. We start with a short Sec. II where we specify the setup, the distribution function we evaluate in the article, and clarify the notations. After this, there are three ways to read the paper depending on reader's interests.

A reader who is eager to see the concrete distributions would first check our numerical results that we produced at various timescales and in parameter regimes demonstrating the possibility of very detailed predictions of continuous weak linear measurement distributions. One would start with the description of the concrete setup (Sec. V). In Sec. VIII we present numerical simulations at time intervals that are much smaller than the typical timescales of all Hamiltonian dynamics focusing on three relevant cases: the case of ideal detectors, and the experimentally relevant case with and without detuning. In Sec. IX, we concentrate on timescales of the order of the decoherence time, inspecting the three cases for ideal detectors with and without drive, and for experimentally relevant setup.

A reader who would like to understand the nontrivial quantum signatures in the distribution would first address the analytical results. In Sec. VI we concentrate on short measuring time intervals and compute the quasidistribution of the shifts of the joint distribution $P(\mathcal{O}_1, \mathcal{O}_2)$, revealing the circle shape mentioned above. In Sec. VII we concentrate on the case of zero overlap between initial and final states and derive analytical expressions for the joint distribution $P(\mathcal{O}_1, \mathcal{O}_2)$ of measurement outcomes in the limit of short time intervals. In this regime, the joint distribution is essentially non-Gaussian and manifests the anomalously big cumulants (*sudden jumps*) in the integrated outputs.

Finally, a methodologically inclined reader would like to start with Sec. III where we outline and develop the necessary formalism to compute the distributions, starting from a Bloch master equation for the qubit evolution that is augmented with counting fields to describe the statistics of detector readouts, and understand the general noises and susceptibilities (Sec. IV). This formalism has been elaborated in our previous work [25]; we extend it here to the simultaneous measurement of two noncommuting variables. There, we discuss the role of various experimental parameters and formulate the relevant quantum noise inequalities for a general multiple detector

setup (Sec. IV). After this, one can go to the concrete results. We conclude in Sec. X.

II. FORMULATION OF THE PROBLEM

Let us consider a quantum system embedded into an environment. As far as the coupling between the system degrees of freedom and those of the environment is weak, the environment can be regarded as a linear one. Let us consider two detectors associated with environmental variables $\hat{V}_i$, $i = 1, 2$. The average values of the detector outputs are proportional to the averages of two quantum system variables $\hat{\mathcal{O}}_i$,

$$\langle \hat{V}_i \rangle = a_{VQ}^{(i,i)} \langle \hat{\mathcal{O}}_i \rangle. \tag{1}$$

Therefore, we simultaneously measure two quantum variables that generally do not commute.

The realistic detectors are noisy and an instant detector reading $V_i(t)$ fluctuates in time. The measurement results may only be relevant if the detector readings are averaged over a time interval. We assume that the measurement is performed during a time interval $(0, \mathcal{T})$. We accumulate the time-dependent outputs and average those over time obtaining the measurement results

$$V_i \equiv \frac{1}{\mathcal{T}} \int_0^{\mathcal{T}} V_i(t) dt. \tag{2}$$

$V_{1,2}$ are still random variables. If we repeat the same measurement, with the same initial state of the system, we obtain different readings. Repeating this big number of times, we can characterize the joint probability distribution of the measurement results $P(V_1, V_2)$. It is convenient to normalize the measurement results introducing the rescaled outputs $\mathcal{O}_i = V_i / a_{VQ}^{(i,i)}$ that immediately correspond to the eigenvalues of $\hat{\mathcal{O}}_i$, and, equivalently, consider $P(\mathcal{O}_1, \mathcal{O}_2)$. (We stress that $\mathcal{O}_i$ are coming from the averaging of the environmental operators rather than $\hat{\mathcal{O}}_i$.)

The evaluation of this distribution function and the discussion of its peculiarities is the subject of this article. An extension of this procedure is the postselected quantum dynamics. In this case, we perform a projective measurement on the quantum system in the end of the measurement, and select the measurement results only if the projective measurement indicates that the quantum system is in the state $|\Psi\rangle$. So, we also consider the so-postselected distribution function $P(\mathcal{O}_1, \mathcal{O}_2)$.

For all concrete examples in the article, the quantum system is a qubit and $\hat{\mathcal{O}}_{1,2}$ correspond to Pauli matrices $\sigma_{x,y}$. With the techniques described in the article one can evaluate more complex distribution functions. For instance, one can separate the measurement interval into smaller parts, and get the joint distribution of the results accumulated during all parts, that reflects the time correlations of the measurements.

III. METHOD

The goal of this section is to introduce a method to efficiently evaluate the probability distributions defined in the previous section. From a variety of possible methods, we use the one first introduced in [24], adjusted to quantum measurement problems in [6], and later extended in [25] to compute the probability distributions of a continuous measurement for a postselected quantum evolution.

In contrast to other possible methods such as path-integral formulation [6,7], effective action method [2,8], past states formalism [23], or the stochastic update equation [27]; this method permits the direct evaluation of the *generating function* of the probability distributions. The parameters $\chi_{1,2}$ of this generating function are customarily called the counting fields since the method originates from the problematics of full counting statistics of electron transport [24].

The central object in the method is a time-dependent quasi-density matrix $\rho(t)$ in the space of the quantum system that depends on $\chi_{1,2}$. The generating function without postselection is expressed as the trace of this matrix at the end of the measurement time interval,

$$C(\chi_1, \chi_2) = \mathrm{Tr}[\rho(\mathcal{T})], \tag{3}$$

and the distribution function is expressed as

$$P(V_1, V_2) = \frac{\mathcal{T}}{2\pi} \int d\chi_1 d\chi_2 e^{-i(\chi_1 V_1 + \chi_2 V_2)\mathcal{T}} C(\chi_1, \chi_2). \tag{4}$$

The evolution of the quasi-density matrix is determined by a Bloch master equation that is augmented with the counting fields. Let us give this equation for a simultaneous measurement of two variables $\hat{\mathcal{O}}_{1,2}$ of the quantum system. We also assume that all decoherence comes from the coupling of the environmental modes with $\hat{\mathcal{O}}_{1,2}$ and the detectors are independent. With this, the equation reads as

$$\frac{\partial \hat{\rho}}{\partial t} = -\frac{i}{\hbar}[\hat{H}_q, \hat{\rho}] - \sum_i \frac{S_{QQ}^{(i,i)}}{\hbar^2} \mathcal{D}[\hat{\mathcal{O}}_i]\hat{\rho} - \frac{\chi_i^2(t)}{2} S_{VV}^{(i,i)} \hat{\rho} - \frac{S_{QV}^{(i,i)}}{\hbar} \chi_i(t) [\hat{\rho}, \hat{\mathcal{O}}_i] + \frac{i a_{VQ}^{i,i} \chi_i(t)}{2} [\hat{\rho}, \hat{\mathcal{O}}_i]_+. \tag{5}$$

Here, $[\ldots,\ldots]$ and $[\ldots,\ldots]_+$ refer to commutator and anticommutator, respectively, $\mathcal{D}[\hat{A}]\hat{\rho} \equiv (\frac{1}{2}[\hat{A}^\dagger \hat{A}, \hat{\rho}]_+ - \hat{A}\hat{\rho}\hat{A}^\dagger)$ and $i = 1, 2$. The coefficients S and a in the equation correspond to the noises and susceptibilities, discussed in Sec. IV in detail.

To condition the probability distribution on the initial state of the quantum system, one uses the initial density matrix $\hat{\rho}(0)$ as the initial condition for Eq. (5). To condition, or postselect, it on the final state, one employs the postselection of the system in a specific state $|\Psi\rangle$ at the time moment $\mathcal{T}$. This involves the projection on the state $|\Psi\rangle$, represented by the projection operator $\hat{P}_\Psi = |\Psi\rangle\langle\Psi|$. This works if one can organize an accurate and fast projective measurement on a known pure state $|\Psi\rangle$. This is the case of the experimental setup of Ref. [12]. In principle, there can be errors in the postselection. Such errors can also be accounted for in the formalism outlined. To this end, one replaces the projection operator $\hat{P}_\Psi$ with a density-matrix-like Hermitian operator $\hat{\rho}_f$ satisfying $\mathrm{Tr}[\hat{\rho}_f] = 1$. For instance, if after a faulty projection measurement with the result "1" the system is in a orthogonal state $|\Psi_2\rangle$ with probability p_e, the corresponding $\hat{\rho}_f$ reads as

$$\hat{\rho}_f = (1 - p_e)|\Psi_1\rangle\langle\Psi_1| + p_e|\Psi_2\rangle\langle\Psi_2|. \tag{6}$$

Thus, to account for the postselection, the quasi-density matrix is projected with $\hat{\rho}_f$, and the generating function of

the detector outcomes reads as [25]

$$\tilde{C}(\chi_1, \chi_2; \mathcal{T}) = \frac{\mathrm{Tr}(\hat{\rho}_f \hat{\rho}(\chi_1, \chi_2; \mathcal{T}))}{\mathrm{Tr}(\hat{\rho}_f \hat{\rho}(\chi_1 = 0, \chi_2 = 0; \mathcal{T}))}. \tag{7}$$

The probability distribution of the detector outcomes can be then computed from the generating function with Eq. (4).

IV. NOISES AND SUSCEPTIBILITIES

For each variable $\hat{\mathcal{O}}_i$, there are two associated variables, input $\hat{Q}_i$ and output $\hat{V}_i$, that are operators in environmental degrees of freedom. The variable $\hat{V}_i$ gives the output of the corresponding detector, and the input variable enters the Hamiltonian as a coupling to the environment $H_{\mathrm{coup}} = -\hat{\mathcal{O}}_i \hat{Q}_i$. The noises S and susceptibilities a entering Eq. (5) are the two-point correlators of these input-output operators:

$$S_{QQ}^{(i,j)} = \frac{1}{2}\int_{-\infty}^{t} dt' \langle\langle \hat{Q}_i(t)\hat{Q}_j(t') + \hat{Q}_j(t')\hat{Q}_i(t)\rangle\rangle, \tag{8a}$$

$$*S_{QV}^{(i,j)} = \frac{1}{2}\int_{-\infty}^{t} dt' \langle\langle \hat{Q}_i(t)\hat{V}_j(t') + \hat{V}_j(t')\hat{Q}_i(t)\rangle\rangle, \tag{8b}$$

$$*S_{VV}^{(i,j)} = \frac{1}{2}\int_{-\infty}^{t} dt' \langle\langle \hat{V}_i(t)\hat{V}_j(t') + \hat{V}_j(t')\hat{V}_i(t)\rangle\rangle, \tag{8c}$$

$$*a_{VQ}^{(i,j)} = -\frac{i}{\hbar}\int_{-\infty}^{t} dt' \langle[\hat{V}_i(t), \hat{Q}_j(t')]\rangle, \tag{8d}$$

$$*a_{QV}^{(i,j)} = -\frac{i}{\hbar}\int_{-\infty}^{t} dt' \langle[\hat{Q}_i(t), \hat{V}_j(t')]\rangle. \tag{8e}$$

This set of noise and response functions define completely the characteristics of the measurement process. Conforming to the assumption of slow qubit dynamics, the noises are white and the responses are instant, corresponding to zero-frequency correlators, at the timescale of Eq. (5).

It is important that the values of these noises and responses are restricted by a set of Cauchy-Schwartz inequalities of the following form [28]:

$$S_{QQ}^{(i,i)} S_{VV}^{(j,j)} - \left|S_{QV}^{(i,j)}\right|^2 \geqslant \frac{\hbar^2}{4}\left|a_{VQ}^{(j,i)} - a_{QV}^{(i,j)}\right|^2, \tag{9}$$

for each pair of operators $\hat{Q}_i, \hat{V}_j$ including $j = i$.

As discussed in [25], these inequalities impose the necessary conditions for the positivity of the probability distributions of measurement outputs. However, it is possible and necessary to derive a more restrictive set of inequalities that impose the conditions for this positivity. In the two-detector case at hand, such extra restriction reads as

$$\begin{aligned} S_{QQ}^{(1,1)} + S_{QQ}^{(2,2)} \geqslant{}& \frac{\hbar^2}{4}\frac{\left|a_{VQ}^{(1,1)} - a_{QV}^{(1,1)}\right|^2}{S_{VV}^{(1,1)}} + \frac{\left|S_{QV}^{(1,1)}\right|^2}{S_{VV}^{(1,1)}} + \frac{\hbar^2}{4}\frac{\left|a_{VQ}^{(2,2)} - a_{QV}^{(2,2)}\right|^2}{S_{VV}^{(2,2)}} + \frac{\left|S_{QV}^{(2,2)}\right|^2}{S_{VV}^{(2,2)}} \\ &+ \hbar\left|\frac{\left(a_{VQ}^{(1,1)} - a_{QV}^{(1,1)}\right)S_{QV}^{(2,1)}}{S_{VV}^{(1,1)}} - \frac{\left(a_{VQ}^{(2,2)} - a_{QV}^{(2,2)}\right)S_{QV}^{(1,2)}}{S_{VV}^{(2,2)}}\right| + \frac{\left|S_{QV}^{(2,1)}\right|^2}{S_{VV}^{(1,1)}} + \frac{\left|S_{QV}^{(1,2)}\right|^2}{S_{VV}^{(2,2)}}. \end{aligned} \tag{10}$$

We demonstrate in the Appendix how to derive such inequalities from analytical expressions of the joint distribution of measurement outcomes. Those and more complex inequalities can be derived from the positivity of the matrix $S_{\beta\alpha} + i\frac{a_{\beta\alpha} - a_{\alpha\beta}}{2}$ where the indices α, β index the whole set of operators $\hat{V}, \hat{Q}$.

V. CONCRETE SETUP

Let us focus on an experimental situation similar to the one in [12], where a transmon qubit with two levels $|e\rangle$, $|g\rangle$ has been embedded in a 3D superconducting cavity split and put under conditions of strong resonant drive that compensates the splitting of the qubit levels. The effective Hamiltonian in the basis of $|e\rangle$, $|g\rangle$ reads as follows:

$$\hat{H}_q = \frac{\hbar}{2}\Omega\hat{\sigma}_x + \frac{\hbar}{2}\Delta\hat{\sigma}_z, \tag{11}$$

Ω being the Rabi frequency proportional to the amplitude of the resonant drive, and Δ being the detuning of the drive frequency from the qubit energy splitting. The interaction with the environment induces decoherence, excitation, and relaxation of the qubit, with the rates $\gamma_d, \gamma_\uparrow, \gamma_\downarrow$, respectively. The measured quantities are related to the fluorescence signal emitted from the qubit.

This is the case of heterodyne detection. The signal from $\sigma_{x,y}$ eventually oscillates at frequency Ω. The accumulating signal is obtained by the mixture of this signal with the resonant drive. Its real and imaginary parts are proportional to the values of σ_x and σ_y, respectively. We associate $\mathcal{O}_1$ and $\mathcal{O}_2$ with these matrices. Equation (5) needs to be adjusted to the case of heterodyne detection. The symmetrized noises S_{VV} have to be taken at frequency Ω rather than on zero frequency. The same pertains the susceptibilities. The most important change concerns the second term in Eq. (5) that, for $\mathcal{O}_{1,2} = \sigma_{x,y}$, describes the decoherence and transitions between the states $\sigma_z|Z^\pm\rangle = \pm|Z^\pm\rangle$. In Eq. (5), the rates of these transitions are equal for both directions, $\gamma_\downarrow = \gamma_\uparrow$. For the case of heterodyne detection, they are not: there are two rates with gaining or losing energy proportional to the quantum noise S_{QQ} at positive and negative frequencies $\pm\Omega$. We also need to add the terms describing the decoherence of the states $|Z^\pm\rangle$.

With this, the equation governing the dynamics $\hat{\rho}(\chi_1, \chi_2)$ reads as

$$\begin{aligned} \frac{\partial\hat{\rho}}{\partial t} = {}& -\frac{i}{\hbar}[\hat{H}_q, \hat{\rho}] - \gamma_d\mathcal{D}[\hat{\sigma}_z]\hat{\rho} - \gamma_\uparrow\mathcal{D}[\hat{\sigma}_+]\hat{\rho} \\ & - \gamma_\downarrow\mathcal{D}[\hat{\sigma}_-]\hat{\rho} - \frac{S_{QV}^{(1,1)}}{\hbar}\chi_1(t)[\hat{\rho}, \sigma_x] \\ & - \frac{S_{QV}^{(2,2)}}{\hbar}\chi_2(t)[\hat{\rho}, \sigma_y] + \frac{ia_{VQ}^{(1,1)}}{2}\chi_1(t)[\hat{\rho}, \sigma_x]_+ \\ & + \frac{ia_{VQ}^{(1,1)}}{2}\chi_2(t)[\hat{\rho}, \sigma_y] - \left(\frac{\chi_1^2(t)}{2}S_{VV}^{(1,1)} + \frac{\chi_2^2(t)}{2}S_{VV}^{(2,2)}\right)\hat{\rho}, \end{aligned} \tag{12}$$

$\hat{\sigma}_+$ ($\hat{\sigma}_-$) being the rising and lowering operators of the qubit, and $\hat{\sigma}_z = |e\rangle\langle e| - |g\rangle\langle g|$ the standard Pauli operator.

All the parameters entering the equation can be characterized from experimental measurements. We provide an example of concrete values in Sec. VIII.

For simplicity, we concentrate on the case of identical and independent detectors where there are no cross noises and susceptibilities and the diagonal noises and susceptibilities are the same for both detectors. In this case, the inequality (9) reads as

$$S_{QQ}S_{VV} - |S_{QV}|^2 \geqslant \frac{\hbar^2}{4}|a_{VQ} - a_{QV}|^2. \tag{13}$$

For a simple system like a single qubit, it is natural to make the measured operator dimensionless, with eigenvalues of the order of one, or, even better, ± 1. With this, one can define and relate the measurement induced dephasing rate $2\gamma = 2S_{QQ}/\hbar^2$ and the acquisition time $t_a \equiv 4S_{VV}/|a_{VQ}|^2$ required to measure the variable $\mathcal{O}_{1,2}$ with a relative accuracy $\simeq 1$.

VI. QUASIDISTRIBUTION OF SHIFTS

For a sufficiently long measurement, the distribution of the measurement results is a shifted Gaussian with the value of the shift proportional to the averaged value of the operator measured. In this case, the spread of the Gaussian is much smaller than the shift. In this section, we will attempt to understand the shifts in the limit of short measurement times $\mathcal{T}$. In principle, any distribution of a vector variable $P(\vec{\mathcal{O}})$ can be presented as a convolution of a Gaussian distribution P_G and a quasidistribution of the shifts:

$$P(\vec{\mathcal{O}}) = \int d\vec{s}\, C(\vec{s}) P_G(\vec{\mathcal{O}} - \vec{s}). \tag{14}$$

One should only not be confused with the fact that $C(\vec{s})$ is a quasidistribution and should not be ever positively defined.

The convolution of such kind is especially natural since the solution of Eq. (5) is proportional to the characteristic function of the Gaussian distribution. If we neglect the cross noises, and the Hamiltonian dynamics, the solution at short $\mathcal{T}$ can be represented as

$$\hat{\rho}(\mathcal{T}) = \exp\left(-\frac{\mathcal{T}\chi_i^2(t)}{2} S_{VV}^{(i,i)}\right)\hat{U}\hat{\rho}(0)\hat{U} \tag{15}$$

with $\hat{U} = \exp\left(\frac{i\mathcal{T}}{2}[a_{VQ}^{1,1}\chi_1\sigma_x + a_{VQ}^{2,2}\chi_2\sigma_x]\right)$. The first factor here is the characteristic function of the Gaussian distribution generated by the detector noises. From the second factor, assuming the initial density matrix $\hat{\rho}_i$ and the postselection described by $\hat{\rho}_f$, we obtain the generating function of the shift quasidistribution

$$C(\vec{\chi}) = \frac{\mathrm{Tr}[\hat{\rho}_f\hat{U}\hat{\rho}_i\hat{U}]}{\mathrm{Tr}[\hat{\rho}_f\hat{\rho}_i]}. \tag{16}$$

We illustrate the quasidistribution of the shifts for the case of a qubit. Although in this paper we concentrate on two-detector setups, it is much more instructive to consider now *three* detectors measuring all three Pauli matrices $\vec{\sigma} = (\sigma_x, \sigma_y, \sigma_z)$. We normalize the detector outputs on ± 1 of Pauli matrix eigenvalues and rescale the corresponding counting fields $\vec{\chi}$ accordingly. With this, the matrix $\hat{U}$ becomes nicely symmetric

$$\hat{U} = \exp[-i(\vec{\chi}, \vec{\sigma})/2]. \tag{17}$$

The final and initial density matrices for a qubit are represented as

$$\hat{\rho}_{i,f} = \tfrac{1}{2}[1 + (\vec{P}_{i,f}, \vec{\sigma})] \tag{18}$$

with polarization vectors $|\vec{P}_{i,f}| < 1$. The generation function for smaller number of detectors is obtained by setting some components of $\vec{\chi}$ to 0. For instance, setting $\chi_{z,y} = 0$ gives

$$C(\chi_x) = (1 + (\vec{P}_i, \vec{P}_f))^{-1}\big(\big[(\vec{P}_i, \vec{P}_f) - P_i^x P_f^x\big] + \big(1 + P_i^x P_f^x\big)\cos\chi_x + i\big(P_i^x + P_f^x\big)\sin\chi_x\big) \tag{19}$$

which corresponds to the following quasidistribution of the shifts"

$$C(s_x) = p_1\delta(s_x - 1) + p_0\delta(s_x) + p_{-1}\delta(s_x + 1), \tag{20}$$

where

$$p_{\pm 1} = \frac{(1 \pm P_i^x)(1 \pm P_f^x)}{2[1 + (\vec{P}_i, \vec{P}_f)]}, \quad p_0 = 1 - p_1 - p_{-1}. \tag{21}$$

This quasidistribution, as discussed in [25], is located on a compact support of half-sums of the eigenvalues ± 1 of the operator σ_x. The half-quantized value $s_x = 0$ is manifested only in the case of postselected measurements.

Multiplying the matrices and taking the trace, we obtain the answer for three detectors. It can be naturally separated into scalar, vector, and tensor parts ($\chi \equiv |\vec{\chi}|$):

$$C_s(\vec{\chi}) = \cos\chi + (\vec{P}_i, \vec{P}_f), \tag{22}$$

$$C_v(\vec{\chi}) = i(\vec{P}_i + \vec{P}_f, \chi)\frac{\sin\chi}{\chi}, \tag{23}$$

$$C_t(\vec{\chi}) = -(\vec{P}_i, \vec{\chi})(\vec{P}_f, \vec{\chi})\frac{2\sin^2(\chi/2)}{\chi^2}, \tag{24}$$

$$C = \frac{C_s + C_v + C_t}{1 + (\vec{P}_i, \vec{P}_f)}. \tag{25}$$

Let us now compute the quasidistribution of the shifts of the inverse Fourier transform of C:

$$C(\vec{s}) = \int \frac{d\vec{s}}{(2\pi)^3} C(\vec{\chi})\exp[-i(\vec{s}, \vec{\chi})]. \tag{26}$$

Eventually, the integral is rather involved. The best way to perform the integration is to try the direct transform. We note that

$$\frac{\sin(\chi A)}{\chi} \equiv z(A) = \int d\vec{s}\frac{\delta(s - A)}{4\pi A}\exp[i(\vec{s}, \vec{\chi})] \tag{27}$$

at any A and

$$\frac{\sin(\chi)}{\chi}, \ \cos(\xi) = \lim_{A\to 1} z(A), \ \frac{d}{dA}z; \tag{28}$$

$$\frac{2\sin^2(\chi/2)}{\chi^2} = \int_0^1 dA\, z(A). \tag{29}$$

With using this we arrive at the quasidistribution of the form

$$C_s(\vec{s}) = -\frac{1}{4\pi}(\delta(s-1)+\delta'(s-1)) + (\vec{P}_i,\vec{P}_f)\delta(\vec{n}), \quad (30)$$

$$C_v(\vec{n}) = -\left(\vec{P}_i+\vec{P}_f,\frac{\partial}{\partial\vec{s}}\right)\delta(s-1), \quad (31)$$

$$C_t(\vec{n}) = \left(\vec{P}_i,\frac{\partial}{\partial\vec{s}}\right)\left(\vec{P}_f,\frac{\partial}{\partial\vec{s}}\right)\frac{\Theta(1-s)}{s}, \quad (32)$$

$$C = \frac{C_s+C_v+C_t}{1+(\vec{P}_i,\vec{P}_f)}. \quad (33)$$

We observe that the vector and tensor contributions provide a quasidistribution located on a compact support $s=0$ or 1. The latter is rather surprising: it invokes a notion of a "classical" qubit spin, a classical unit vector pointing in an arbitrary direction. While for such classical spin the quasidistribution would have been positive, this is not the case of actual quantum mechanical expression: the quasidistribution is made of δ function and its derivatives. We do not find it instructive to plot the resulting quasidistribution. The tensor part also contains terms located on this support. In addition, there are terms $\propto(\vec{P}_f,\vec{s})(\vec{P}_i,\vec{s})/s^5$ located within the sphere $s<1$. The tensor part persists only for the case of postselected measurement $\vec{P}_f\neq 0$.

To obtain the distribution of two outputs, we integrate it over s_z making use of

$$\int ds_z z(A) = \frac{2}{\sqrt{A^2-s_\perp^2}}, \quad s_\perp \equiv \sqrt{s_x^2+s_y^2}. \quad (34)$$

The resulting quasidistribution reads as (here, the indices $a,b=x,y$)

$$C_s(\vec{s}) = -\frac{1}{2\pi}\frac{1}{(1-s_\perp^2)^{3/2}} + (\vec{P}_i,\vec{P}_f)\delta(s_x)\delta(s_y), \quad (35)$$

$$C_v(\vec{s}) = -\left(P_i^a+P_f^a,\frac{\partial}{\partial n^a}\right)\delta(s-1), \quad (36)$$

$$C_t(\vec{s}) = P_i^a\frac{\partial}{\partial s^a}P_f^b\frac{\partial}{\partial s^b}\operatorname{arccosh}(s_\perp^{-1}), \quad (37)$$

$$C = \frac{C_s+C_v+C_t}{1+(\vec{P}_i,\vec{P}_f)}. \quad (38)$$

We see that this quasidistribution is located at the compact support $s_x^2+s_y^2=1$, $s_x^2+s_y^2=0$ as well as inside the circle $s_x^2+s_y^2<1$. This gives us an expectation that the actual distribution of the measurement results should exhibit some peculiarities at $s_x^2+s_y^2=1$, an expectation that is confirmed by numerical results of subsequent sections.

It is worth noting that the generalized functions involved in the quasidistributions presented in Eqs. (38) and (33) are rather involved and should be dealt with carefully. In particular, a direct attempt to integrate Eq. (38) over n_y does not immediately reproduce Eq. (20) as it should. Rather, the integration diverges near $s_x^2+s_y^2=1$. To resolve this apparent paradox, one requires a regularization of the generalized functions involved. Such regularization can be provided by replacing

$$\delta(s-A) \to \pi^{-1}\operatorname{Im}\frac{1}{A+i\xi} \quad (39)$$

at small but finite ξ. With this, the divergence at the circle edge is eliminated and Eq. (20) is reproduced.

VII. SHORT TIME INTERVALS AND ZERO OVERLAP

In this section, we also concentrate on very short $\mathcal{T}$ such that the change of the density matrix due to Hamiltonian and dissipative dynamics is small. Since the measuring time is too short to resolve the signal with sufficient accuracy, we expect the distribution to be close to the Gaussian one

$$P_G(\mathcal{O}_1,\mathcal{O}_2) = \prod_{i=1,2}\frac{1}{\sigma_i\sqrt{2\pi}}\exp\left(-\frac{\mathcal{O}_i^2}{2\sigma_i^2}\right), \quad (40)$$

with $\sigma_i^2 = S_{VV}^{(i,i)}/(\mathcal{T}|a_{VQ}^{(i,i)}|^2)$. The spread of $\mathcal{O}$ is much larger than their eigenvalues. However, the distribution can become quite different if the overlap between the initial state $|i\rangle$ and the final state of the projective measurement $|\Psi\rangle$ vanishes: $\langle i|\Psi\rangle\to 0$. The latter implies that such output of the projective measurement is very improbable. Nevertheless, such outcomes can be singled out and their statistics are worth studying.

A peculiarity termed a *sudden jump* of the integrated output is characteristic for this situation. It can be explained from the concept of weak values [21] as far as average outputs are concerned. For the whole statistics of the outputs, the sudden jump was studied for a single-variable measurement [25]. Here, we demonstrate that the sudden jump is also seen in the statistics of simultaneous measurement of two variables. A proper choice of Hamiltonian permits for a simultaneous sudden jump in both integrated outputs. The signature of sudden jump is enhanced in the distribution where the distribution of one output is conditioned on a specific value of another one.

To this end, let us first focus at the experimental situation of [12]. In this case, the two measured variables are conveniently chosen to be $\hat{\sigma}_x$ and $\hat{\sigma}_y$ and the qubit is driven by a Hamiltonian $\hat{H}_q = \hbar\frac{\Omega}{2}\hat{\sigma}_x$. In the simplest case where the two detectors are independent and no cross noises are present, and with the assumptions of short $\mathcal{T}$ and zero overlap $\langle i|\Psi\rangle=0$ (the qubit is prepared in $|Z^+\rangle$ and postselected in $|Z^-\rangle$), one obtains the following joint characteristic function of the distribution of detector outputs:

$$C(\chi,\mathcal{T}) = \frac{4\gamma+\mathcal{T}\left[\left(\Omega-ia_{VQ}^{(2,2)}\chi_2\right)^2-\left(a_{VQ}^{(1,1)}\chi_1\right)^2\right]}{4\gamma+\mathcal{T}\Omega^2}e^{-\frac{1}{2}\sum_i S_{VV}^{(i,i)}\chi_i^2\mathcal{T}}, \quad (41)$$

$\gamma = S_{QQ}^{(1,1)}/\hbar^2 + S_{QQ}^{(2,2)}/\hbar^2$ being the decoherence rate.

This gives the average outputs

$$\bar{\mathcal{O}}_1 = 0, \quad \bar{\mathcal{O}}_2 = -\frac{2\Omega}{4\gamma + \mathcal{T}\Omega^2}, \tag{42}$$

and the joint distribution

$$P(\mathcal{O}_1, \mathcal{O}_2) = \frac{1}{4\gamma + \mathcal{T}\Omega^2}\left\{4\gamma + \mathcal{T}\left[\left(\Omega - \frac{4\mathcal{O}_2}{t_{a2}}\right)^2 - \frac{4}{\mathcal{T}t_{a2}} + \frac{4}{t_{a1}}\left(\frac{4\mathcal{O}_1^2}{t_{a1}} - \frac{1}{\mathcal{T}}\right)\right]\right\} P_G(\mathcal{O}_1, \mathcal{O}_2). \tag{43}$$

The value of average output $\bar{\mathcal{O}}_2$ thus saturates at $-\Omega/2\gamma \ll -1$ in the limit of short $\mathcal{T} \ll \gamma/\Omega^2$. Note that this sudden jump behavior, at a timescale of γ/Ω^2, now is only visible at the time-integrated output of the variable $\mathcal{O}_2$ not commuting with the Hamiltonian. Thus, to achieve a simultaneous sudden jump for both time-integrated outputs, we need to require that the Hamiltonian does not commute with both variables. Let us modify the Hamiltonian to $\hat{H}_q = \hbar\frac{\Omega_x}{2}\hat{\sigma}_x + \hbar\frac{\Omega_y}{2}\hat{\sigma}_y$. The joint characteristic function can be written as

$$C(\chi, \mathcal{T}) = \frac{4\gamma + \mathcal{T}\left[\left(\Omega_x - ia_{VQ}^{(2,2)}\chi_2\right)^2 - \left(i\Omega_y - a_{VQ}^{(1,1)}\chi_1\right)^2\right]}{4\gamma + \mathcal{T}\bar{\Omega}^2} e^{-\frac{1}{2}\sum_i S_{VV}^{(i,i)}\chi_i^2\mathcal{T}}, \tag{44}$$

where $\bar{\Omega}^2 = (\Omega_x^2 + \Omega_y^2)$. This gives the average outputs

$$\bar{\mathcal{O}}_1 = \frac{2\Omega_y}{4\gamma + \mathcal{T}\bar{\Omega}^2}, \quad \bar{\mathcal{O}}_2 = -\frac{2\Omega_x}{4\gamma + \mathcal{T}\bar{\Omega}^2}. \tag{45}$$

Therefore, both time-integrated outputs exhibit a sudden jump at a timescale of $\gamma/\bar{\Omega}^2$. The joint probability distribution of measurement outcomes can then be computed by Fourier transformation of the joint characteristic function (44), and is given by

$$P(\mathcal{O}_1, \mathcal{O}_2) = \frac{1}{4\gamma + \mathcal{T}\bar{\Omega}^2}\left\{4\gamma + \mathcal{T}\left[\left(\Omega_x - \frac{4\mathcal{O}_2}{t_{a2}}\right)^2 + \left(\Omega_y + \frac{4\mathcal{O}_1}{t_{a1}}\right)^2 - \frac{4}{\mathcal{T}t_{a2}} - \frac{4}{\mathcal{T}t_{a1}}\right]\right\} P_G(\mathcal{O}_1, \mathcal{O}_2). \tag{46}$$

Here, $t_{ai} \equiv 4S_{VV}^{(i,i)}/|a_{VQ}^{i,i}|^2$ are the acquisition times corresponding to each detector.

For the simplest case of identical but independent detectors $t_{a1} = t_{a2}$, this distribution is positive as long as $K \equiv \gamma t_a \geqslant 1$ ($K = 1$ corresponding to an ideal detector), which is always guaranteed by the corresponding Cauchy-Schwartz inequality (13).

It is instructive to inspect the forms of the distributions (43) and (46) to understand the main characteristics of such a measurement scenario. We do that by plotting the joint distributions and several cross sections of these joint distributions, that is, the plots of the probability density in one variable at fixed value of another one. In Figs. 1 and 2 we present these two distributions for a measurement time $\mathcal{T} = 4/\Omega^2 t_a$ and $4/\bar{\Omega}^2 t_a$, respectively. The first plot, Fig. 1(a), presents the joint distribution covering a huge range of detector outcomes due to the short measurement time $\mathcal{T}$. The sudden jump behavior of the integrated output is visible at this timescale. The position of the peaks and the average integrated outputs in the $(\mathcal{O}_1, \mathcal{O}_2)$ plane for these distributions depend only on the choice of the Hamiltonian dynamics, as can be seen by comparing Figs. 1 and 2.

In Figs. 1(b) and 1(c) we present the cross sections of the joint distribution (43). First, due to the asymmetry of the Hamiltonian with respect to the two detector outputs, the distributions for $\mathcal{O}_1$ [Fig. 1(a)] are intrinsically different than the distributions for $\mathcal{O}_2$ [Fig. 1(b)]. While the average value of the integrated output $\mathcal{O}_1$ corresponding to the measurement

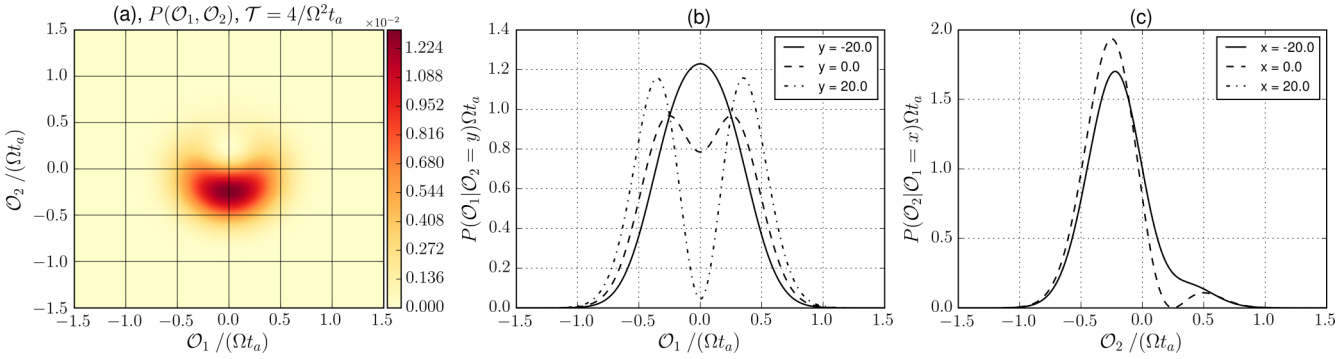

FIG. 1. (a) Probability distribution of outputs [Eq. (43)] in the sudden jump regime in case of an ideal detector ($K \equiv \gamma t_a = 1$). (b), (c) Present postselected distributions. In (b), we plot the probability distribution of $\mathcal{O}_1$ output given a $\mathcal{O}_2 = y$ result for the other output. (c) Gives the probability distribution of $\mathcal{O}_2$ output given a $\mathcal{O}_1 = x$ result for the other output. All distributions are evaluated at $\mathcal{T} = 4/(\Omega^2 t_a)$.

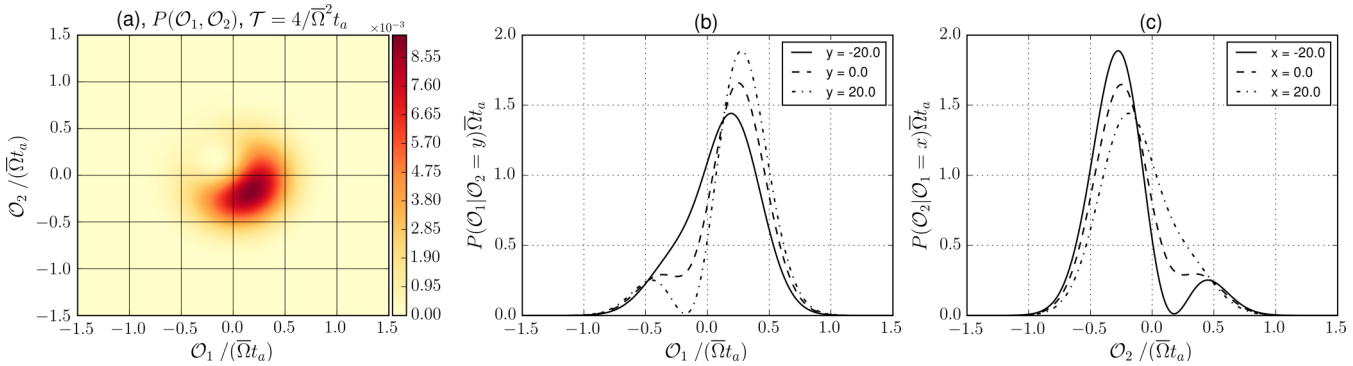

FIG. 2. (a) Probability distribution of outputs [Eq. (46)] in the sudden jump regime in case of an ideal detector ($K \equiv \gamma t_a = 1$). (b), (c) Present postselected distributions. (b) Gives the probability distribution of $\mathcal{O}_1$ output given a $\mathcal{O}_2 = y$ result for the other output. (c) Gives the probability distribution of $\mathcal{O}_2$ output given a $\mathcal{O}_1 = x$ result for the other output. All the distributions are evaluated at $\mathcal{T} = 4/(\bar{\Omega}^2 t_a)$. We set $\Omega_x = \Omega_y$, this explains the symmetry.

of $\hat{\mathcal{O}}_1 = \hat{\sigma}_x$ is zero, the average integrated output of the second variable $\hat{\mathcal{O}}_2 = \hat{\sigma}_y$ can reach anomalously big values as explained by theory of weak values [21]. Figure 1(b) also shows how conditioning on results of the second integrated output can be used to drastically change the distribution of the first integrated output, going from a noise-dominated distribution (full line curve for $\mathcal{O}_2 = -20$) to a well-resolved measurement (dashed-dotted curve for $\mathcal{O}_2 = 20$).

As noted above, with a proper choice of Hamiltonian, one can achieve anomalously large average integrated outputs in both variables. Thus, now using $\hat{H}_q = \hbar\frac{\Omega_x}{2}\hat{\sigma}_x + \hbar\frac{\Omega_y}{2}\hat{\sigma}_y$, in Figs. 2(b) and 2(c) we present cross sections of the joint distribution (46). Here, the asymmetry between the two distributions 2(a) and 2(b) disappears and the maximum and minimum values are the same due to our choice of parameters ($\Omega_x = \Omega_y$).

In the Appendix, we use the analytical results for the distribution in the limit of short time and zero overlap to check the positivity of the distribution of measurement outcomes for a more general set of detector noises and responses. We show that the positivity of the distribution is guaranteed provided the inequality (10) is fulfilled.

VIII. NUMERICAL RESULTS: SHORT TIMESCALES

In this section, we numerically evaluate the full probability distribution of measurement outcomes in the same regime as in the previous section, but for experimental conditions. The measurement time is short compared to the Hamiltonian dynamics of our qubit and the state of the measured system does not vary significantly during this measurement time. For simplicity, in the remainder of this paper we will always consider vanishing cross noises, $S_{QV}^{(i,i)} = 0$, for a set of identical but independent detectors. This is not restrictive since the numerical evaluations can be readily extended to any experimental situation involving the continuous measurement of two variables.

In our numerical studies, both for short time intervals in this section and longer time intervals in Sec. IX, we will focus on three cases:

(i) An ideal detection case, where we numerically solve Eq. (5) with $\hat{H}_q = \hbar\frac{\Omega}{2}\hat{\sigma}_x$ and parameter values such that the inequality (13) becomes an equality. This implies that all the decoherence arises from the detectors back-action and their rates assume the minimum permitted values $K = t_a\gamma = 1$.

(ii) An experimentally relevant case, where we numerically solve Eq. (12) with $\hat{H}_q = \hbar\frac{\Omega}{2}\hat{\sigma}_x$, $\gamma_\downarrow = (22.5\ \mu\text{s})^{-1}$, $\gamma_\uparrow = (56\ \mu\text{s})^{-1}$, and $\gamma_d = (15.6\ \mu\text{s})^{-1}$. The acquisition time comes from the measurement rate $2/t_a \approx (92\ \mu\text{s})^{-1}$ as given in [12].

(iii) Another experimentally relevant case, that differs by including a substantial detuning $\Delta \approx 1.7\Omega$ to the Hamiltonian $\hat{H}_q = \hbar\frac{\Omega}{2}\hat{\sigma}_x + \hbar\frac{\Delta}{2}\hat{\sigma}_z$. This value of the detuning is chosen to maximize $\langle\mathcal{O}_1\rangle$ for the equilibrium density matrix.

The distributions of the measurements for these three cases are presented in three different figures: Fig. 3 for the ideal case, and Figs. 4 and 5 for no and substantial detuning, respectively. In these three figures, we plot the joint distribution for different combinations of initial and final (postselected) states of the measured qubit. We also present the cross sections of this distribution, that is, the distribution of a particular detector output at a given output of another detector. The first row of plots, (a), (b), and (c), presents these distributions for a qubit prepared in $|Z^+\rangle$ and postselected after the measurement in $|Z^+\rangle$; we refer to this as P_+. The second row of plots, (d), (e), and (f), presents these distributions for a qubit prepared in $|Z^+\rangle$ and postselected in $|Z^-\rangle$; we refer to this as P_-.

Also, the first column of plots, (a) and (d), presents density plots of the joint distribution of measurement outcomes $[P_+(\mathcal{O}_1,\mathcal{O}_2)$ and $P_-(\mathcal{O}_1,\mathcal{O}_2)]$ for both measured variables and for the measurement time $\mathcal{T} = 0.05\Omega^{-1}$. The second column of plots, (b) and (e), presents different conditioned distributions of the detector output $\mathcal{O}_2$ given specific values $\mathcal{O}_1 = x$ of the other detector output $[P_+(\mathcal{O}_2|\mathcal{O}_1 = x)$ and $P_-(\mathcal{O}_2|\mathcal{O}_1 = x)]$, again for a measurement time $\mathcal{T} = 0.05\Omega^{-1}$. Finally, the third column of plots, (c) and (f), presents different conditioned distributions of the detector output $\mathcal{O}_2$ given a result of $\mathcal{O}_1 = 0$ of the other detector output $[P_+(\mathcal{O}_2|\mathcal{O}_1 = 0)$ and $P_-(\mathcal{O}_2|\mathcal{O}_1 = 0)]$ for different measurement times $\mathcal{T} = 0.05, 0.2, 0.5\Omega^{-1}$.

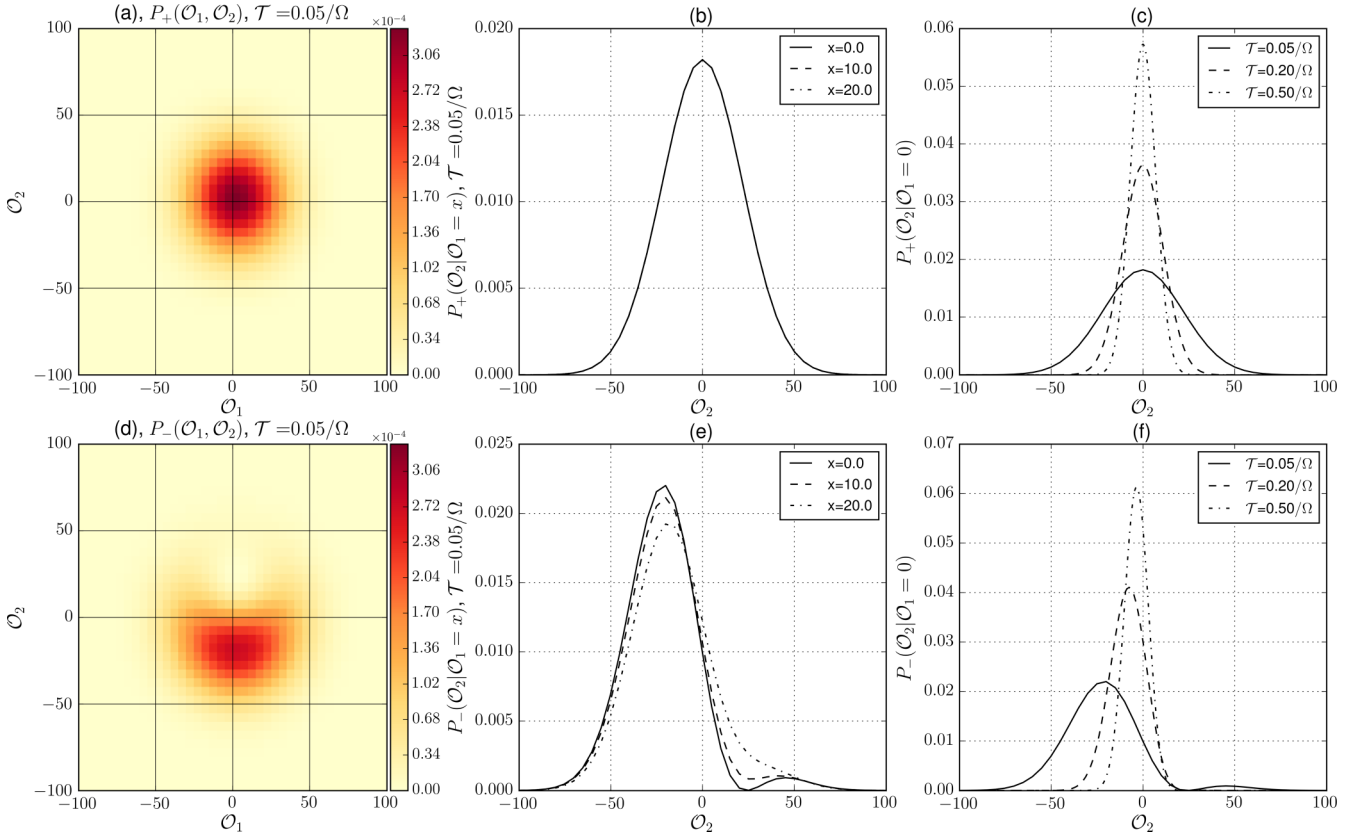

FIG. 3. Output distributions for the simultaneous measurement of $\hat{\mathcal{O}}_1=\hat{\sigma}_x$ and $\hat{\mathcal{O}}_2=\hat{\sigma}_y$. The measurement with ideal detectors [case (i)] for $\mathcal{T}\ll\Omega^{-1}$ or comparable with Ω^{-1}. The qubit is prepared in $|Z^+\rangle$ and postselected at the end of the measurement: in $|Z^+\rangle$ for the first row of figures [plots (a)–(c)]; and in $|Z^-\rangle$ for the second row of figures [plots (d)–(f)].

At these short measurement times, one expects these distributions to be duly Gaussian spreading over a large range of detector output values. This is seen in the upper row of plots. As we have shown previously, there is only one particular case where this is not true: the case of vanishing overlap between the initial and postselection states. A sudden jump behavior in the averaged integrated output is illustrated in the second row of plots in Figs. 3, 4, and 5, manifested in these figures as very non-Gaussian distribution shapes. In these numerical results, one sees small deviations from analytical predictions at $\mathcal{T}\to 0$ since is $\mathcal{T}$ is finite. The plots show anomalously large values for the average integrated output seen as big shifts in the distribution peaks, in agreement with the analytical results of the previous section. The agreement is visible if one compares Fig. 3(e) with Fig. 1(c).

As expected, this peculiarity is suppressed as the Hamiltonian dynamics starts to be relevant ($\mathcal{T}\sim\Omega^{-1}$) as can be seen in the different curves at increasing time intervals in the third column of plots in Figs. 3, 4, and 5. The shape of the distributions becomes more Gaussian as the detectors considered are less ideal. This can be seen when comparing the distributions for ideal detectors (Fig. 3) and experimentally relevant parameters (Figs. 4 and 5).

As the measurement time is short compared to the Hamiltonian dynamics, the qubit state changes insignificantly during the measurement. This fact is manifested in the sudden jump behavior of the P_- distributions in the second row of plots, and in the fact that Figs. 4 and 5 are almost the same. At these short measurement times, a difference in the Hamiltonian is not noticeable.

IX. NUMERICAL RESULTS: LONGER TIMESCALES

In the previous section, we have presented the distributions of continuous weak linear measurement outcomes of the simultaneous measurement of two noncommuting variables in the limit of short measurement times. In this section, we address the distributions of the continuous weak linear measurement outcomes of the simultaneous measurement of two noncommuting variables at timescales of the order of coherence and relaxation times and t_a.

To begin with, let us assume no Hamiltonian and ideal detectors [case (i) with no Hamiltonian]. With this, the postselected distribution of outcomes changes only at the timescale $t_a\simeq\gamma^{-1}$, that is much longer than Ω^{-1}, and the dynamics are described by Eq. (5) with vanishing $S_{QV}^{(i,i)}$ and $\hat{H}_q$ terms.

As discussed in Sec. VI, the preselection and postselection condition leads to peculiarities in the joint distribution that are located around the circle $\mathcal{O}_1^2+\mathcal{O}_2^2=1$. These peculiarities should be visible in these conditions, at intermediate measurement times that are longer than Ω^{-1} but short enough so that they are comparable to $t_a\simeq\gamma^{-1}$.

In fact, this is what we present in Fig. 6 when plotting the joint distributions [first column of plots, (a), (d), and (g)]. The cross sections [(b), (e) and (h); and (c), (f), and (i)] show the expected half-quantization peculiarities characteristic of a

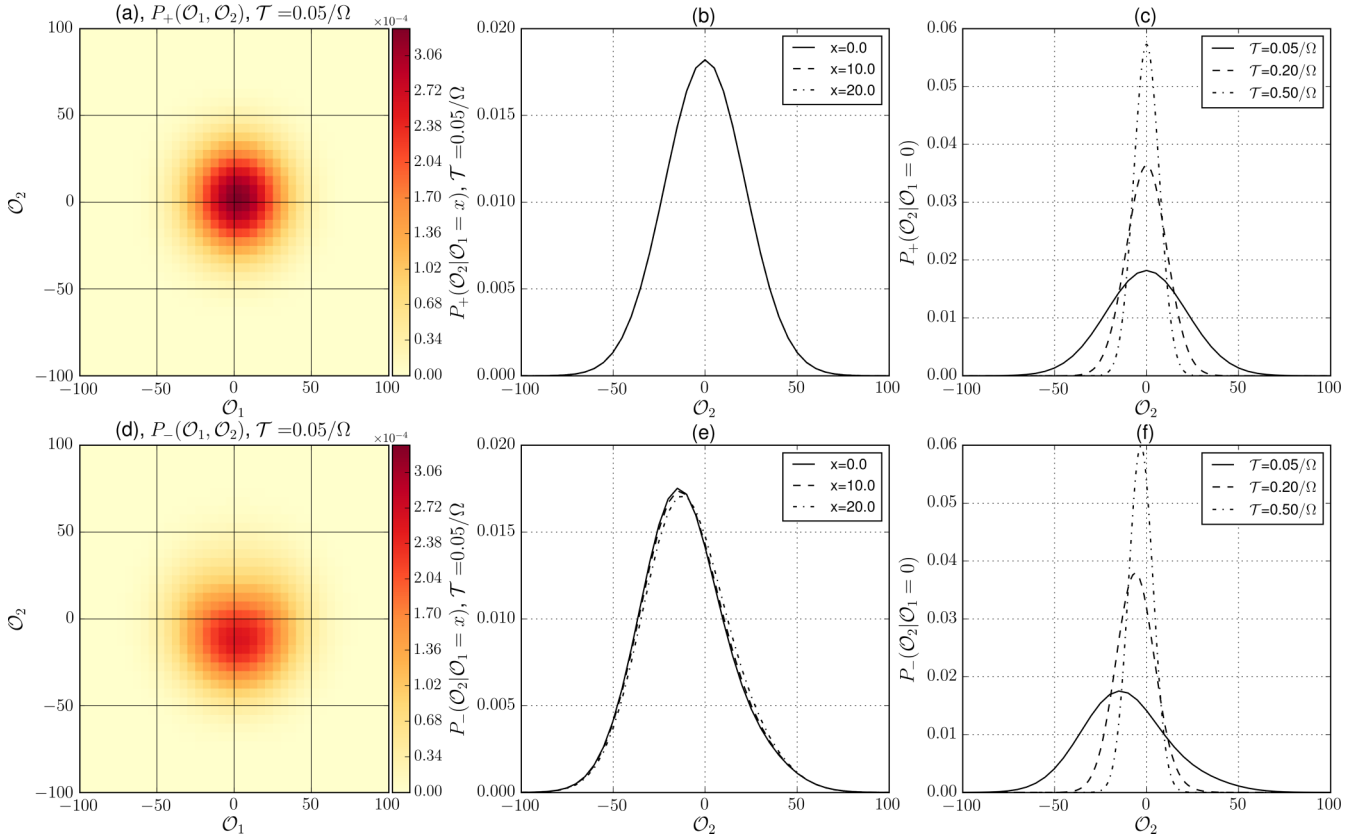

FIG. 4. The measurement with nonideal detectors and experimentally relevant parameters [case (ii)]. The qubit is prepared in $|Z^+\rangle$ and postselected at the end of the measurement: in $|Z^+\rangle$ state for the first row of figures [plots (a)–(c)]; and in $|Z^-\rangle$ for the second row of figures [plots (d)–(f)].

single-variable measurement, extensively discussed in [25]. In the last column of plots [(c), (f), and (i)] one could expect the separation of the distribution onto peaks at the limit $\mathcal{T} \gg t_a$. However, this is a signature of a quantum nondemolition measurement, and the fact that we inspect the simultaneous measurement of two noncommuting variables means that the measurement itself will induce rates causing transitions between the qubit states and therefore is not a nondemolition measurement.

It is worth mentioning that the fact that all these distributions are symmetric under a change $\mathcal{O}_1 \leftrightarrow \mathcal{O}_2$ is due to the choice identical detectors and no Hamiltonian dynamics in any of those variables axes ($\hat{\mathcal{O}}_1 = \hat{\sigma}_x$ and $\hat{\mathcal{O}}_2 = \hat{\sigma}_y$).

To explain these observations, let us describe precisely the layout both for Figs. 6 and 7: the (a) plots show the joint distribution of measurement outcomes $P_+(\mathcal{O}_1, \mathcal{O}_2)$ for a qubit prepared in $|Z^+\rangle$ and postselected in the same state after the measurement of duration $\mathcal{T} = 0.4t_a$. The (d) plots show the joint distribution of measurement outcomes $P_-(\mathcal{O}_1, \mathcal{O}_2)$ for a qubit prepared in $|Z^+\rangle$ and postselected in the orthogonal state $|Z^-\rangle$ after the measurement of duration $\mathcal{T} = 0.4t_a$. The (g) plots show the joint distribution of measurement outcomes $P(\mathcal{O}_1, \mathcal{O}_2)$ for a qubit prepared in $|Z^+\rangle$ unconditioned to any postselection after the measurement of duration $\mathcal{T} = 0.4t_a$. Next, in the second column, the (b) plots present the conditioned distributions $P_+(\mathcal{O}_1|\mathcal{O}_2 = y)$ of the first output, given a result $\mathcal{O}_2 = y$ for the second output, again for a qubit prepared in $|Z^+\rangle$ and postselected in the same state after the measurement of duration $\mathcal{T} = 0.4t_a$. Respectively, the (e) and (h) plots show the conditioned distributions $P_-(\mathcal{O}_1|\mathcal{O}_2 = y)$ and $P(\mathcal{O}_1|\mathcal{O}_2 = y)$. Finally, in the third column, we plot the conditioned distributions $P_+(\mathcal{O}_1|\mathcal{O}_2 = 0)$ in (c), $P_-(\mathcal{O}_1|\mathcal{O}_2 = 0)$ in (f), and $P(\mathcal{O}_1|\mathcal{O}_2 = 0)$ in (i); for different measurement duration $\mathcal{T} = 0.4, 0.8, 1.2t_a$.

In contrast with the figures of the previous section, the measurement time is big enough for the qubit state to change appreciably during the measurement. This is why we also plot the unconditioned distributions $P(\mathcal{O}_1, \mathcal{O}_2)$ now being clearly different from the distributions conditioned to a specific postselection $P_\pm(\mathcal{O}_1, \mathcal{O}_2)$.

Let us incorporate Hamiltonian dynamics to this measurement scenario, focusing now on the case (i). If we keep the final state fixed to $|Z^\pm\rangle$, the contribution due to the postselected evolution in these distributions will exhibit fast oscillations as function of $\mathcal{T}$ with a period $2\pi/\Omega$. It is proficient from both theoretical and experimental considerations to quench these rather trivial oscillations. We achieve this by projecting the qubit after the measurement on the states $|\bar{Z}^\pm\rangle = e^{-i\hat{H}_q\mathcal{T}}|Z^\pm\rangle$, thereby correcting for the trivial qubit dynamics. In practice, such correction can be achieved by applying a short pulse rotating the qubit about the x axis right before the postselection measurement.

With this, the asymmetry in the Hamiltonian with respect to the measured $\hat{\mathcal{O}}_1$ and $\hat{\mathcal{O}}_2$ variables will break the symmetry in the shape of the distributions. Then, the conditioned distributions for the output $\mathcal{O}_2$ are just Gaussian functions

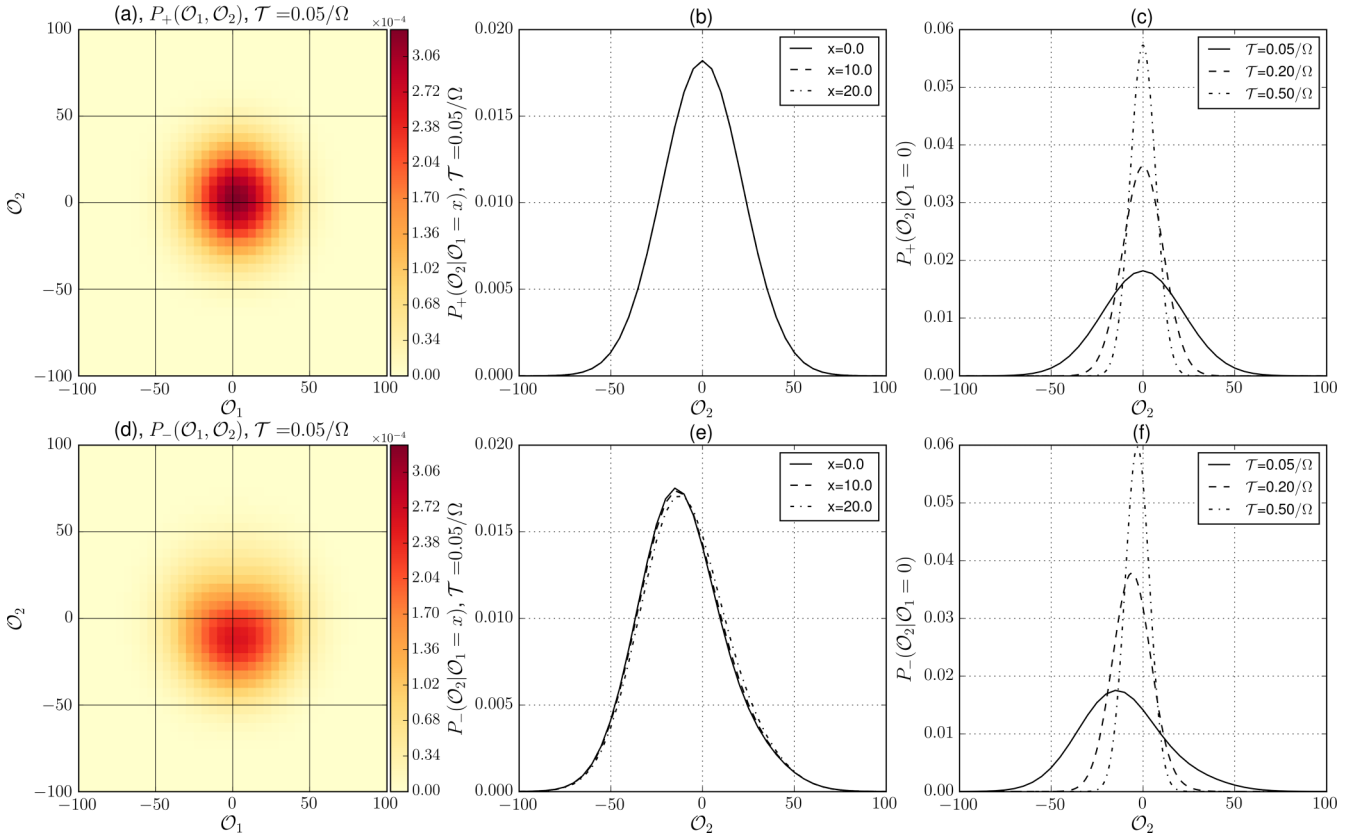

FIG. 5. The measurement with nonideal detectors and strong detuning [case (iii)]. The qubit is prepared in $|Z^+\rangle$ and postselected at the end of the measurement: in $|Z^+\rangle$ for the first row of figures [plots (a)–(c)]; and in $|Z^-\rangle$ for the second row of figures [plots (d)–(f)].

centered at $\mathcal{O}_2 = 0$ with their spread decreasing over time as $\sim 1/\sqrt{\mathcal{T}}$. Therefore, they give no information about the output $\mathcal{O}_2$ at this timescale. That is why we choose to plot the conditioned distributions for the output $\mathcal{O}_1$. This situation is presented in Fig. 7. The choice of Hamiltonian now collapses all these peculiarities due to the preselection and postselection conditions in one of the two outputs. This is clearly manifested in the shape of the joint distributions [Figs. 7(a), 7(d), and 7(g)]. A similar effect is produced by the addition of dynamics to the measured qubit: this results in a clear and strong suppression of the dependence of a given output on the other output outcomes as can be seen in Figs. 7(b), 7(e), and 7(h). Finally, if one compares the time evolution of these distributions [plots (c), (f), and (i)] for Figs. 6 and 7, the addition of dynamics to the measured qubit results in a less resolved measurement, that is, for a given measurement time $\mathcal{T}$ the dynamics decreases the separation of the peaks.

Although this shows that the interference effect and peculiarities due to postselected evolution are still visible at longer timescales for an ideal measurement scenario, it is also clear that these signatures are suppressed by dynamics of the measured qubit. In fact, in an experimental situation, where external sources of decoherence are present, resolving those signatures might become a very challenging task. It is then important to inspect an experimentally relevant parameter regime in these numerical simulations.

To this end, one can inspect experimentally relevant scenarios: the cases (ii) and (iii). It is worth noting that the quality of the measurement setup in these conditions is far from ideal, $K = t_a\gamma_d \approx 12$, and, at longer timescales, the decoherence completely dominates all the measurement dynamics. It is so that the distributions do not show apparent characteristics of the postselected qubit evolution: they are close to just Gaussian distributions centered at zero value of the outcome variables.

In this case, it is instructive to inspect the difference of two particular distributions, rather than the distribution itself. With this in mind, in Figs. 8 and 9 we plot various differences of distributions. In Figs. 8 and 9 we concentrate on cases (ii) and (iii), correspondingly. We investigate the postselected measurements as well as the unselected ones, and look at statistics of a single variable as well as the joint statistics.

These two figures are structured as follows: The (a) plots show the difference of the distribution of the first output disregarding the second output and the distribution of the same first output given a specific result y for the second output $P_+(\mathcal{O}_1) - P_+(\mathcal{O}_1|\mathcal{O}_2 = y)$. The (b) plots show the same difference divided by its sum $[P_+(\mathcal{O}_1) - P_+(\mathcal{O}_1|\mathcal{O}_2 = y)]/[P_+(\mathcal{O}_1) + P_+(\mathcal{O}_1|\mathcal{O}_2 = y)]$, both for a qubit prepared in $|Z^+\rangle$ state and postselected in the same state. The (c) plots again show this difference but for a qubit prepared in $|Z^+\rangle$ and postselected in $|Z^-\rangle$, i.e., $P_-(\mathcal{O}_1) - P_-(\mathcal{O}_1|\mathcal{O}_2 = y)$. Respectively, the plots (d) show that difference divided by the sum $[P_-(\mathcal{O}_1) - P_-|(\mathcal{O}_1|\mathcal{O}_2 = y)]/[P_-(\mathcal{O}_1) + P_-(\mathcal{O}_1|\mathcal{O}_2 = y)]$. These differences give an estimation of the correlation between the two outputs in these measurements, or the separability of the joint distribution.

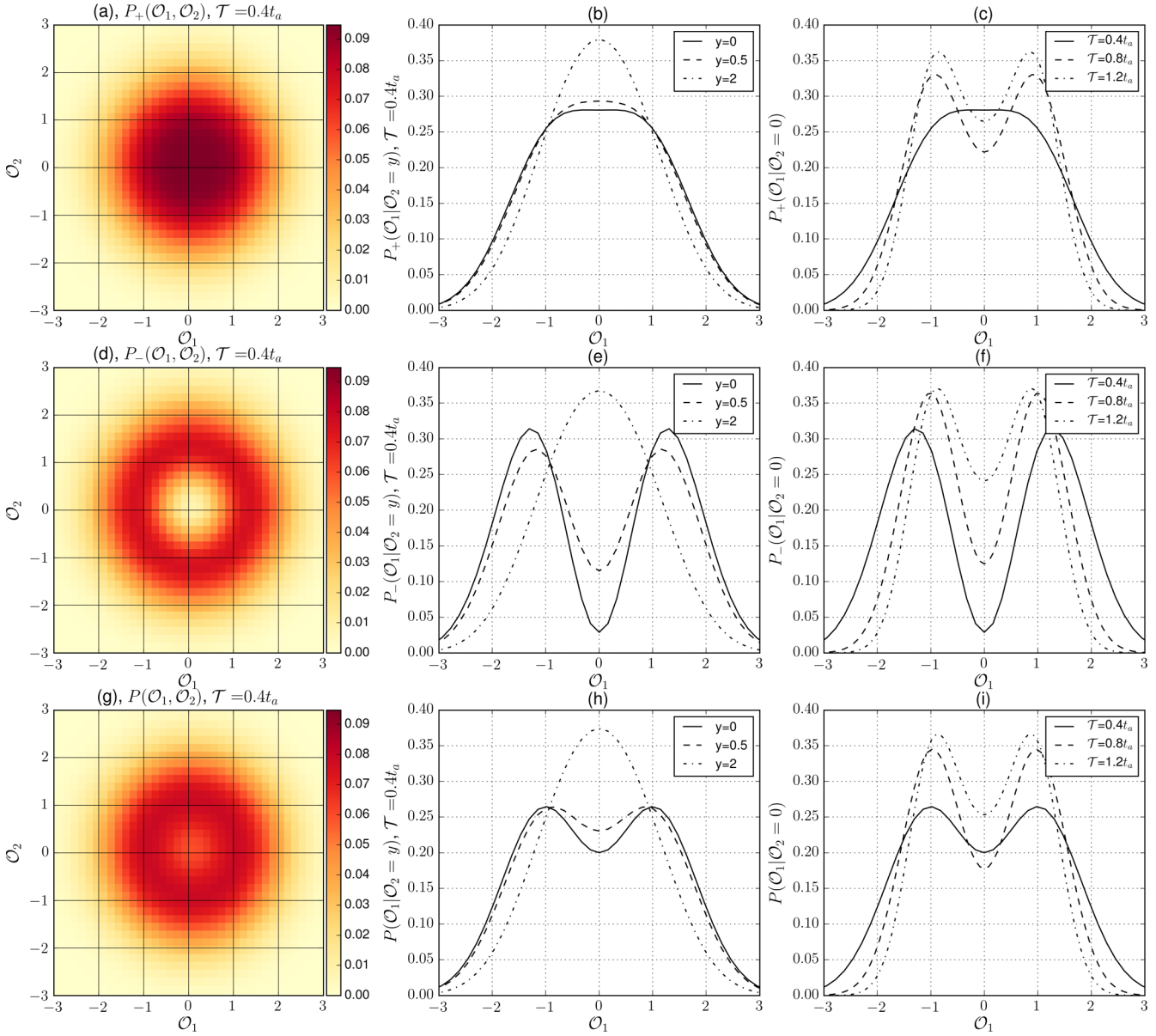

FIG. 6. Output distributions for the simultaneous measurement of $\hat{\mathcal{O}}_1=\hat{\sigma}_x$ and $\hat{\mathcal{O}}_2=\hat{\sigma}_y$. The qubit is prepared in $|Z^+\rangle$ and postselected either in $|Z^+\rangle$ for the first row of figures [plots (a), (b), and (c)]; or in $|Z^-\rangle$ for the second row of figures [plots (d), (e), and (f)]. There is no postselection for the last row of figures [plots (g), (h), and (i)]. The measurement is performed with ideal detectors and no Hamiltonian dynamics are present during time intervals comparable to the acquisition time of the measurement setup. In this configuration, the peculiarities discussed in Sec. VI are clearly visible in the joint distributions [plots (a), (d), and (g)].

Next, the plots (e) show the difference between the distribution of the first output given a specific result y for the second output for a qubit prepared in $|Z^+\rangle$ and postselected in the same state, and the distribution of the first output given a specific result y for the second output for a qubit prepared in $|Z^+\rangle$ and postselected in $|Z^-\rangle$. That is, $P_+(\mathcal{O}_1|\mathcal{O}_2=y)-P_-(\mathcal{O}_1|\mathcal{O}_2=y)$. The plots (f) show this difference divided by their sum $[P_+(\mathcal{O}_1|\mathcal{O}_2=y)-P_-(\mathcal{O}_1|\mathcal{O}_2=y)]/[P_+(\mathcal{O}_1|\mathcal{O}_2=y)+P_-(\mathcal{O}_1|\mathcal{O}_2=y)]$. Finally, the plots (g) show the same difference, but for the distributions of the second output given a specific result x for the first output: $P_+(\mathcal{O}_2|\mathcal{O}_1=x)-P_-(\mathcal{O}_2|\mathcal{O}_1=x)$. Respectively, plots (h) show that difference divided by their sum $[P_+(\mathcal{O}_2|\mathcal{O}_1=x)-P_-(\mathcal{O}_2|\mathcal{O}_1=x)]/[P_+(\mathcal{O}_2|\mathcal{O}_1=x)+P_-(\mathcal{O}_2|\mathcal{O}_1=x)]$. The reason for inspecting the latter differences is simple: we want to quantify the signatures of the postselected evolution. Thus, the comparison of the difference between the two limiting cases of this postselected evolution, same and orthogonal initial and final states, shows how strong these signatures are. Furthermore, the differences divided by the sums quantify to which extent these signatures can be resolved by using the output distributions of such measurements. In other words, this gives the certainty with which one can distinguish two distributions from each other given a measurement reading [25]

$$C(\mathcal{O}_i|\mathcal{O}_j=\alpha)=\frac{P_+(\mathcal{O}_i|\mathcal{O}_j=\alpha)-P_-(\mathcal{O}_i|\mathcal{O}_j=\alpha)}{P_+(\mathcal{O}_i|\mathcal{O}_j=\alpha)+P_-(\mathcal{O}_i|\mathcal{O}_j=\alpha)}. \tag{47}$$

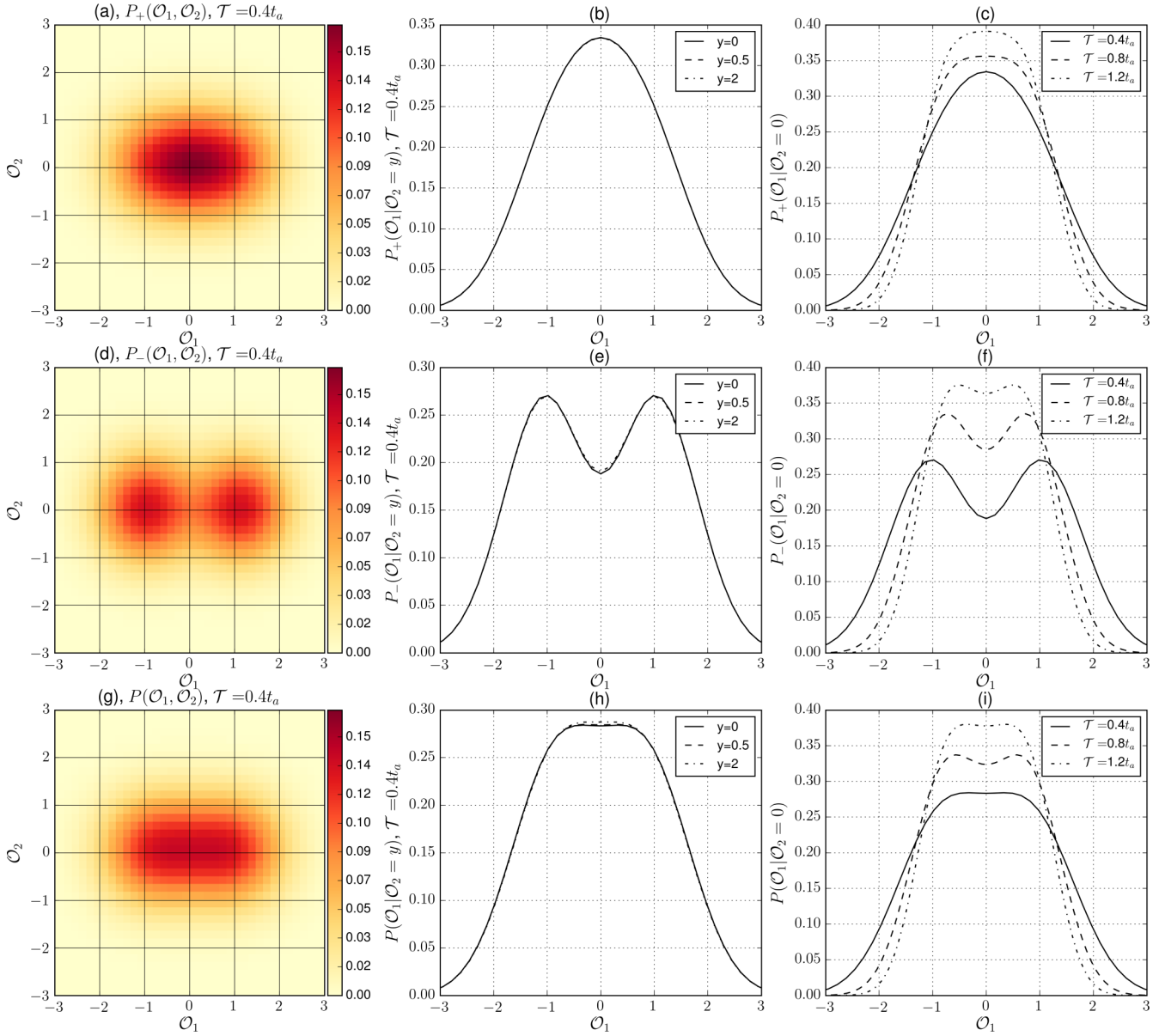

FIG. 7. Here, the output distributions for a measurement performed with ideal detectors [case (i)] during time intervals comparable to the acquisition time of the measurement setup. The Hamiltonian drastically changes the type of peculiarities seen in the distributions. This can be seen by comparison with Fig. 6.

The values $C=\pm 1$ would imply that, at given measurement outcomes, the outcome of the projective measurement is *certainly* $|Z^{\pm}\rangle$.

In this experimental regime at zero detuning, Fig. 8, the differences of distributions 8(a) and 8(c) reveal that the two outputs are still correlated, and this correlation seems to be bigger for given values of the outputs that are farther away from the origin where the distributions peak at such timescales. Nevertheless, it is very small, as the joint distribution quickly becomes a Gaussian due to decoherence and relaxation. At big values of $\mathcal{O}_1$, the difference quickly decreases together with the distributions. In this respect, it is instructive to inspect the difference normalized on the sum of the probability densities. As we see from Figs. 8(b) and 8(d), this quantity increases with increasing $\mathcal{O}_1$, reaches relatively large values at increasing $\mathcal{O}_2=y$ results due to their low statistical weight, and seems to remain relevant at a small region $\mathcal{O}_1\sim 0$ even for big times. This region is more relevant because this quantity is not suppressed or increased due to exponentially low probabilities for those values; it is rather a direct measure of the correlation of the two outputs.

The signatures of the postselected evolution are revealed by the differences in Figs. 8(e) and 8(g). As expected due to the form of the Hamiltonian (on $\hat{\mathcal{O}}_1=\hat{\sigma}_x$ axis), Fig. 8(e) is very different from Fig. 8(g). In Fig. 8(e), the shape of the difference suggests that the $P_-(\mathcal{O}_1|\mathcal{O}_2=y)$ is pushed on both positive and negative values of $\mathcal{O}_1$ in comparison with $P_+(\mathcal{O}_1|\mathcal{O}_2=y)$, in agreement with the previous findings. The decoherence and relaxation quickly diminish the difference upon increasing $\mathcal{T}$. Inspecting the certainty in Fig. 8(f), it saturates with increasing $\mathcal{O}_1$, reaches relatively large values at short $\mathcal{T}$, and fades away upon increasing $\mathcal{T}$. Note that

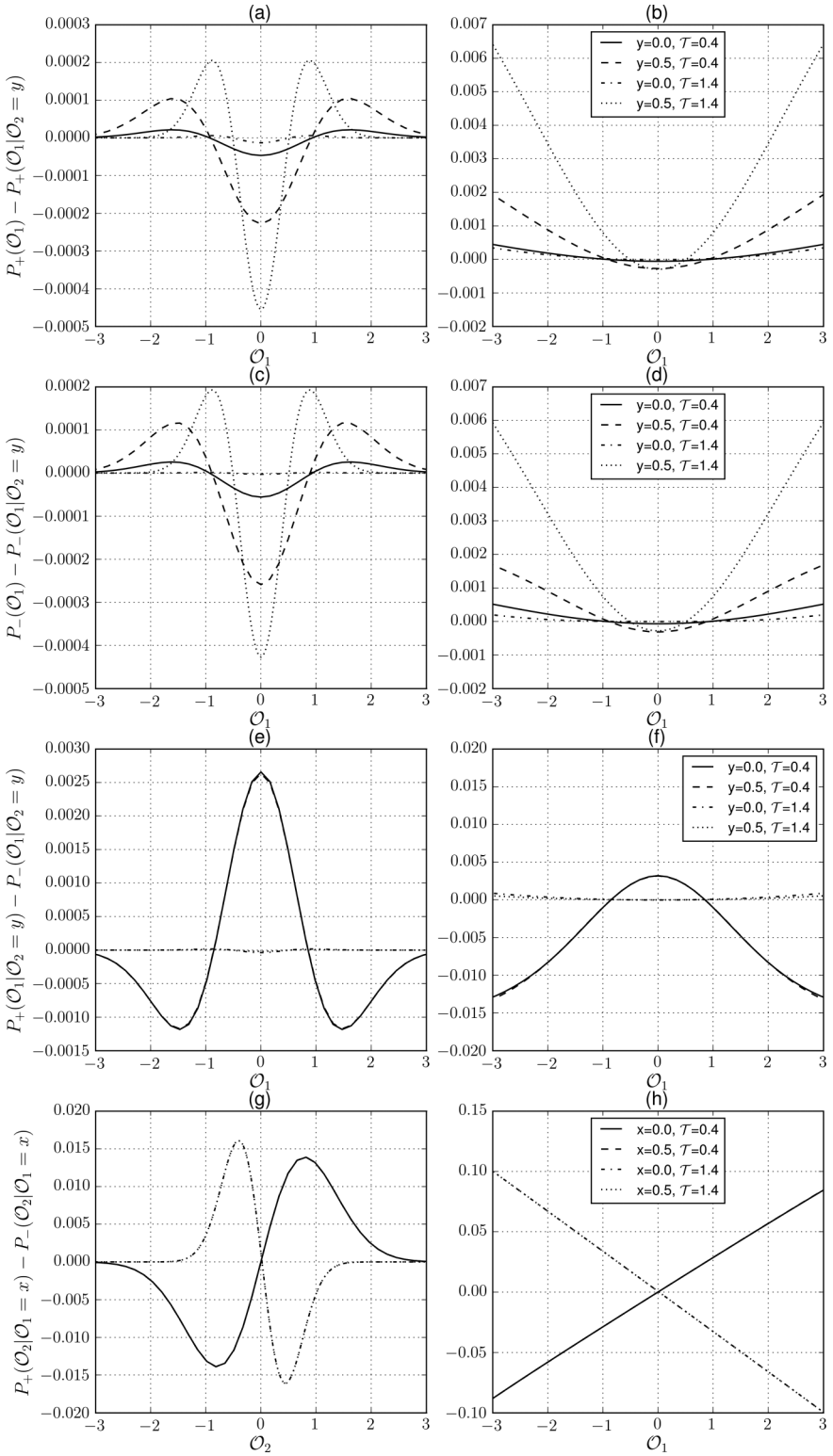

FIG. 8. Differences of distributions at measurement times of the order of the acquisition time t_a under experimentally relevant measurement conditions [case (ii)]. In the first column of plots, different distributions are examined to understand the correlations between outputs and time evolution in (a) and (c), as well as the visibility of the postselected evolution peculiarities in the statistics of both outputs in (e) and (f). In the second column, the plotted difference of probabilities is divided by the sum of the same probabilities. The layout is described in detail in Sec. IX in the main text.

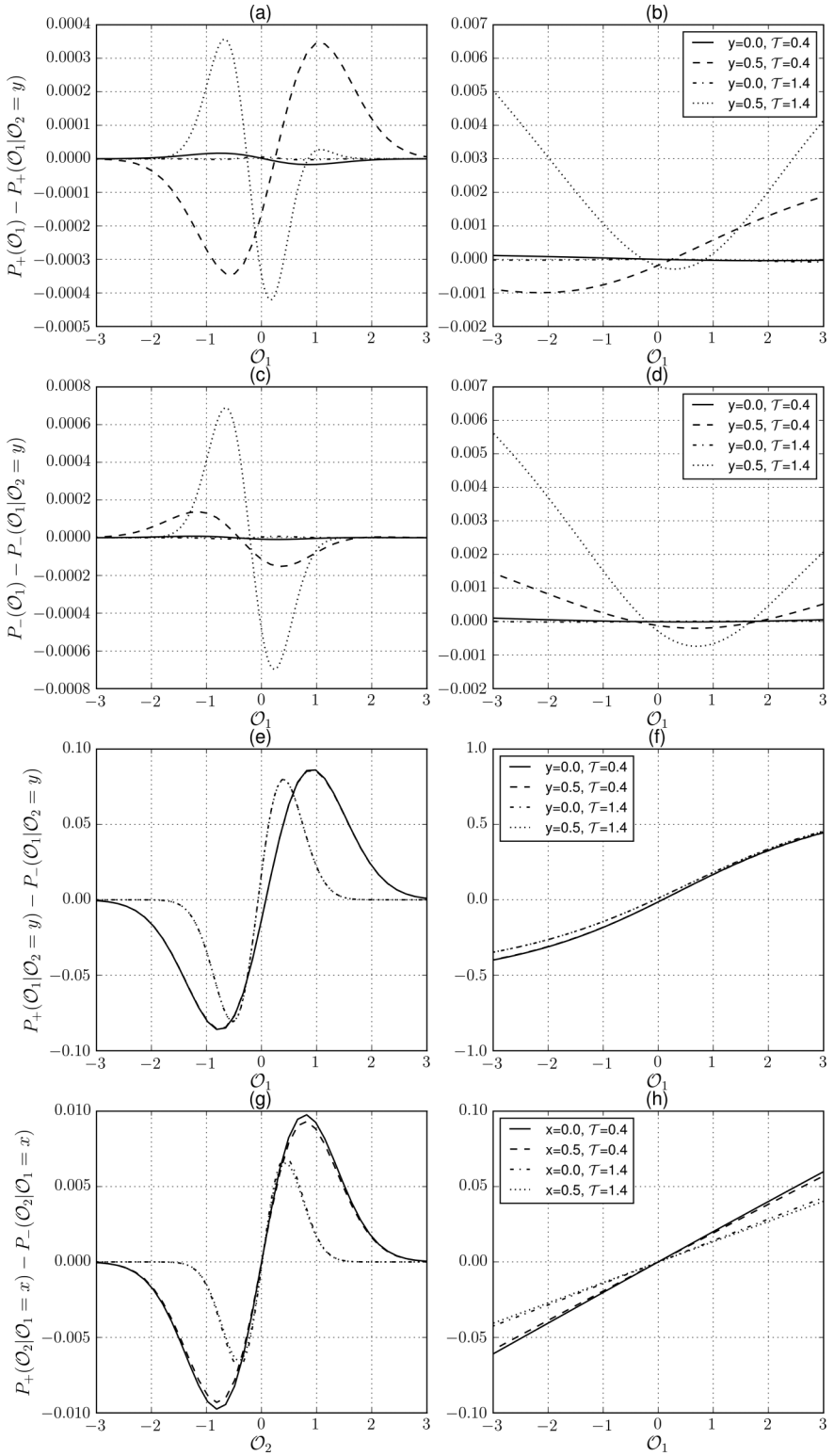

FIG. 9. Differences of distributions taken at measurement times of the order of the acquisition time t_a and at nonzero detuning [case (iii)]. The layout is the same as in Fig. 8.

at short $\mathcal{T} = 0.4t_a$ this relative difference achieves 0.002 at $\mathcal{O}_1 \approx 0$ and can be thus revealed from the statistics of several hundred individual measurements. For the second output $\mathcal{O}_2$, the differences in Fig. 8(g) are an order of magnitude bigger than those for the $\mathcal{O}_1$ distributions in Fig. 8(e). Not only that, but the difference does not vanish in the limit of big $\mathcal{T}$. Rather, it is concentrated in an increasingly narrow interval of $\mathcal{O}_2$ conforming to the decreasing width of the distribution. It is worth noting that they also change sign as $\mathcal{T}$ increases. For short times, the shape of $P_-(\mathcal{O}_2|\mathcal{O}_1 = x)$ resembles the shape of the distribution at the sudden jump regime (Fig. 4), as the time $\mathcal{T}$ increases, the distributions are shifted depending on

the postselected state. This is not the case for the $\mathcal{O}_1$ output discussed previously because of the chosen Hamiltonian. As to the certainty in Fig. 8(h), it shows a linear behavior with $\mathcal{O}_2$, $C(\mathcal{O}_2|\mathcal{O}_1 = x) = \beta\mathcal{O}_2$. The sign of β depends on the sign of the shift in the distributions, and the linear behavior can be explained in the limit of small shifts. This does not imply that the distributions are different in this limit since they become concentrated with divergent probability density, and the values of $\mathcal{O}_2$ that provide the high certainty occur with exponentially low probability. This is discussed in detail in Sec. V of [25].

Let us inspect these differences of distributions at nonzero detuning in Fig. 9. In this case, there is no reason to expect the $\mathcal{O}_1 \to -\mathcal{O}_1$ symmetry in the distributions, nor in their differences. Similar to the previous plots, the differences showed in Figs. 9(a), 9(b), 9(c), and 9(d) reveal the small correlations between the two outputs, now in the presence of detuning. These are bigger when the distributions are conditioned with the bigger values of the outputs. The differences of the probability distributions presented in Figs. 9(e) and 9(g) seem to be at least one order of magnitude bigger than that for the distributions of the first output in Fig. 9(e), compared to the zero detuning case in Fig. 8. We also see that for both outputs, the difference does not vanish in the limit of big $\mathcal{T}$. Rather, it is concentrated in an increasingly narrow interval of $\mathcal{O}_{1,2}$ conforming to the decreasing width of the distribution. This suggests that adding a strong detuning can increase the detection resolution, and reveal these distribution differences from the statistics of fewer individual measurements. However, as mentioned before, the certainties, Figs. 9(f) and 9(g), rather quickly converge upon increasing $\mathcal{T}$ to finite and rather big values in a wide interval of the output $\mathcal{O}_{1,2}$ in question. Once again, this does not imply that the distributions are fundamentally different in this limit since they become concentrated with divergent probability densities. For the certainty of the second output distributions in Fig. 9(h), a linear behavior appears due to the limit of small shifts for these distributions.

Although the joint distribution of measurement outcomes effectively becomes a product distribution $P(\mathcal{O}_1, \mathcal{O}_2) \approx P(\mathcal{O}_1)P(\mathcal{O}_2)$ and the correlations between the two noncommuting variables are lost rather fast upon increasing $\mathcal{T}$, it is worth noting that the signature of interference due to the postselected dynamics in the probability distribution can still be revealed in experimental conditions from the statistics of several hundred individual measurements.

X. CONCLUSION

In this work, we put forward a proper theoretical formalism based on full counting statistics approach [6,24] to describe and evaluate the measurement statistics in the course of postselected quantum evolution. We extend the previous work [25] to the simultaneous measurement of two noncommuting variables. We illustrate this formalism with several examples and prove that the interesting features arising from the postselected quantum evolution can be seen in the statistics of the measurement outcomes for both short and relatively long measurement intervals. We also reveal the interplay between the two noncommuting variables statistics and the signatures of the postselected dynamics in the individual and joint distributions.

We describe and investigate two signatures of the postselected statistics that are related to quantum interference effects. First is the appearance of peculiarities at the circle $\mathcal{O}_1^2 + \mathcal{O}_2^2 = 1$ in the distribution of measurement outcomes, that is revealed by a quasidistribution of shifts located at the compact support $\mathcal{O}_1^2 + \mathcal{O}_2^2 = 1$, $\mathcal{O}_1^2 + \mathcal{O}_2^2 = 0$ as well as inside the circle $\mathcal{O}_1^2 + \mathcal{O}_2^2 < 1$. This provides a connection with what we termed *half-quantized* measurement values for the single-variable measurement case, as the distribution function may display peculiarities, that are either peaks or dips, at half-sums of the quantized values. In the special case of zero overlap between initial and final states and time intervals that are so short as the wave function of the system does not significantly change by either Hamiltonian or dissipative dynamics. We reveal unexpectedly large values of the time-integrated output cumulants for such short intervals, that we termed *sudden jump*. We show that a simultaneous jump in integrated output can be achieved in both measured variables given an appropriate choice of Hamiltonian. This effect is felt in a short timescale γ/Ω^2 where γ^{-1} is the timescale of dissipative dynamics and Ω^{-1} is the timescale of Hamiltonian dynamics. In addition to this, our results show that it is possible to achieve bigger saturation values for these anomalously big averages when further conditioning the statistics of one output with the results of other outputs.

Our results show that it is possible to have very detailed theoretical predictions of continuous weak linear measurement distributions. In particular, we show how to use this formalism to account for postselected quantum evolution and simultaneous noncommuting variable measurements in the paradigm of continuous weak linear measurement. This opens the possibility for investigation and characterization of quantum effects even if the choice of parameters is far from ideal and the effects are small.

The signatures in the distributions that we predict in this paper can be seen in realistic experimental regimes. One of the key elements to experimentally observe this effect is the ability to efficiently record time traces for a weak continuous monitoring of one or rather several qubit variables, and this has been achieved in several papers [9–15,19] applying it for the observation of qubit trajectories or real-time feedback. Thus, we believe it is possible to extract these kind of statistics from the existing records of several experiments.

ACKNOWLEDGMENTS

This work was supported by the Netherlands Organization for Scientific Research (NWO/OCW), as part of the Frontiers of Nanoscience program.

APPENDIX: POSITIVITY OF THE DISTRIBUTION

Here, we present the derivation of the inequality (10) from the analytical procedure used in Sec. VII to derive the joint distribution of measurement outcomes at short times $\mathcal{T}$ and given a vanishing overlap between preparation and postselection states $\langle i|\Psi\rangle = 0$. To do so, we focus first on the simple setup considered in the main text. Next, we add different

correlations between the two detectors, understand what they add to the picture, and derive a more general restriction.

To start with, note that for any pair of operators $\hat{Q}, \hat{V}$ it is possible to construct a Cauchy-Schwarz inequality of the following form [28]:

$$S_{QQ}(\omega)S_{VV}(\omega) - |S_{QV}(\omega)|^2 \geqslant \left|\frac{\hbar}{2}[a_{VQ}(\omega) - a_{QV}(\omega)]\right|^2 \times \left\{1 + \Delta\left[\frac{S_{QV}(\omega)}{\frac{\hbar}{2}[a_{VQ}(\omega) - a_{QV}(\omega)]}\right]\right\}, \tag{A1}$$

where

$$\Delta[z] = [|1 + z^2| - (1 + |z|^2)]/2. \tag{A2}$$

In the limit of zero frequency, this reproduces the inequality (13).

However, in the case where we have more than one detector or measured variable, i.e., more than one pair of input-output variables $\hat{Q}, \hat{V}$, there are additional inequalities restricting the correlators between input-output variables pertaining to these different pairs. An easy way to see this is to inspect the distribution we calculated for short timescales [Eq. (43)]. It describes the case of independent detectors without cross noises. Let us find the conditions for it to be positive at all values of $\mathcal{O}_{1,2}$. This condition reads as

$$\gamma \geqslant \frac{1}{t_{a1}} + \frac{1}{t_{a2}}. \tag{A3}$$

For us, the inequality can be written as

$$S^{(1,1)}_{QQ} + S^{(2,2)}_{QQ} \geqslant \frac{\hbar^2}{4}\left(\frac{|a^{(1,1)}_{VQ}|^2}{S^{(1,1)}_{VV}} + \frac{|a^{(2,2)}_{VQ}|^2}{S^{(2,2)}_{VV}}\right). \tag{A4}$$

We write this assuming the condition of a good amplifier, that is, the direct gain exceeds much the reverse one [28], $a^{(1,1)}_{VQ} \gg a^{(1,1)}_{QV}$. All results presented here can be extended to a more general situation by replacing $a^{(i,i)}_{VQ}$ with the difference $a^{(i,i)}_{VQ} - a^{(i,i)}_{QV}$. This inequality can be constructed as the sum of two inequalities of the form (9) for the two sets of input-output variables involved. This fact explicitly shows that this inequality does not add any more restrictions to the correlators than the ones that come from the aforementioned Cauchy-Schwarz inequalities.

Now, let us derive the distribution at short time for a more general case where the cross noises and correlations are present, and then check the condition for positivity once again. First, for any correlations between output variables, meaning $S^{(1,2)}_{VV} = S^{(2,1)}_{VV} \neq 0$, the distribution (43) will change, however, the condition for positivity will not. In particular, adding correlations between output variables modifies it in the following way:

$$P(\mathcal{O}_1, \mathcal{O}_2) = \frac{1}{4\gamma + \mathcal{T}\bar{\Omega}^2}\left\{4\gamma + \mathcal{T}\left[\left(\Omega_x - \frac{4\mathcal{O}_2}{t_{a2}} - \frac{2\mathcal{O}_1 S^{(1,2)}_{VV}}{a^{(2,2)}_{VQ}a^{(1,1)}_{VQ}}\right)^2 + \left(\Omega_y + \frac{4\mathcal{O}_1}{t_{a1}} + \frac{2\mathcal{O}_2 S^{(1,2)}_{VV}}{a^{(2,2)}_{VQ}a^{(1,1)}_{VQ}}\right)^2 - \frac{4}{\mathcal{T}t_{a2}} - \frac{4}{\mathcal{T}t_{a1}}\right]\right\} P_G(\mathcal{O}_1, \mathcal{O}_2). \tag{A5}$$

The positivity of the distribution is again guaranteed by the same condition (A4). Let us now introduce cross noises between input-output, i.e., $S^{(1,1)}_{QV}, S^{(2,2)}_{QV}, S^{(1,2)}_{QV}, S^{(2,1)}_{QV} \neq 0$. The distribution of measurement outcomes can then be approximated as

$$P(\mathcal{O}_1, \mathcal{O}_2) = \frac{1}{4\gamma + \mathcal{T}\bar{\Omega}^2}\left[4\gamma + \mathcal{T}\left(\left\{\Omega_x + \left(\frac{2S^{(1,2)}_{QV}}{a^{(2,2)}_{V,Q}} - 1\right)\frac{\mathcal{O}_2}{\mathcal{T}\sigma_2^2} + \frac{2S^{(1,1)}_{QV}}{a^{(1,1)}_{V,Q}}\frac{\mathcal{O}_1}{\mathcal{T}\sigma_1^2}\right]^2 + \left[\Omega_y + \left(1 + \frac{2S^{(2,1)}_{QV}}{a^{(1,1)}_{V,Q}}\frac{\mathcal{O}_1}{\mathcal{T}\sigma_1^2}\right) + \frac{2S^{(2,2)}_{QV}}{a^{(2,2)}_{V,Q}}\frac{\mathcal{O}_2}{\mathcal{T}\sigma_2^2}\right]^2 - \left(1 - \frac{2S^{(1,2)}_{QV}}{a^{(2,2)}_{V,Q}}\right)^2\frac{1}{\mathcal{T}^2\sigma_2^2} - \left(\frac{2S^{(1,1)}_{QV}}{a^{(1,1)}_{V,Q}}\right)^2\frac{1}{\mathcal{T}^2\sigma_1^2} - \left(1 + \frac{2S^{(2,1)}_{QV}}{a^{(1,1)}_{V,Q}}\right)^2\frac{1}{\mathcal{T}^2\sigma_1^2} - \left(\frac{2S^{(2,2)}_{QV}}{a^{(2,2)}_{V,Q}}\right)^2\frac{1}{\mathcal{T}^2\sigma_2^2}\right)\right] P_G(\mathcal{O}_1, \mathcal{O}_2). \tag{A6}$$

Here, $\sigma_i^2 = t_{ai}/4\mathcal{T}$. For this distribution to be positive we have the following condition:

$$\gamma - \left(1 - \frac{2S^{(1,2)}_{QV}}{a^{(2,2)}_{V,Q}}\right)^2\frac{1}{t_{a2}} - \left(\frac{2S^{(1,1)}_{QV}}{a^{(1,1)}_{V,Q}}\right)^2\frac{1}{t_{a1}} - \left(1 + \frac{2S^{(2,1)}_{QV}}{a^{(1,1)}_{V,Q}}\right)^2\frac{1}{t_{a1}} - \left(\frac{2S^{(2,2)}_{QV}}{a^{(2,2)}_{V,Q}}\right)^2\frac{1}{t_{a2}} \geqslant 0, \tag{A7}$$

which one can write as

$$S^{(1,1)}_{QQ} + S^{(2,2)}_{QQ} \geqslant \frac{\hbar^2}{4}\left\{\left[\left(a^{(2,2)}_{V,Q} - 2S^{(1,2)}_{QV}\right)^2 + \left(2S^{(2,2)}_{QV}\right)^2\right]\frac{1}{S^{(2,2)}_{VV}} + \left[\left(a^{(1,1)}_{V,Q} + 2S^{(2,1)}_{QV}\right)^2 + \left(2S^{(1,1)}_{QV}\right)^2\right]\frac{1}{S^{(1,1)}_{V,V}}\right\}. \tag{A8}$$

Conversely, if one takes the initial state to be $|Z^-\rangle$ and the final projection to be $|Z^+\rangle$, then the condition becomes

$$S^{(1,1)}_{QQ} + S^{(2,2)}_{QQ} \geqslant \frac{\hbar^2}{4}\left\{\left[\left(a^{(2,2)}_{V,Q} + 2S^{(1,2)}_{QV}\right)^2 + \left(2S^{(2,2)}_{QV}\right)^2\right]\frac{1}{S^{(2,2)}_{VV}} + \left[\left(a^{(1,1)}_{V,Q} - 2S^{(2,1)}_{QV}\right)^2 + \left(2S^{(1,1)}_{QV}\right)^2\right]\frac{1}{S^{(1,1)}_{V,V}}\right\}. \tag{A9}$$

The probability distribution of measurement outcomes should remain positive regardless of the initial and final conditions. Thus, both these inequalities (A8) and (A9) have to be fulfilled. Taking this into account, one can write the inequality (10), where inverse susceptibilities are added back, owing to the possibility of bad amplifiers.

This shows that the existence of cross noises between input-output of different detectors imposes a stronger restriction on the possible values for the set of noises and response functions defining a measurement scenario than the usual Cauchy-Schwarz inequalities considered. It is worth noting that we did not consider nonvanishing responses between input-output of different detectors. The analysis can be extended to this case with even more complex restrictions on the correlators for the positivity of the distribution of measurement outcomes.

[1] M. Nielsen and I. Chuang, *Quantum Computation and Quantum Information* (Cambridge University Press, Cambridge, 2000).

[2] M. B. Mensky, Phys. Lett. A **155**, 229 (1991).

[3] A. N. Korotkov, Phys. Rev. B **60**, 5737 (1999).

[4] A. N. Jordan and M. Büttiker, Phys. Rev. Lett. **95**, 220401 (2005).

[5] K. Jacobs and D. A. Steck, Contemp. Phys. **47**, 279 (2006).

[6] H. Wei and Y. V. Nazarov, Phys. Rev. B **78**, 045308 (2008).

[7] A. Chantasri and A. N. Jordan, Phys. Rev. A **92**, 032125 (2015).

[8] A. Chantasri, J. Dressel, and A. N. Jordan, Phys. Rev. A **88**, 042110 (2013).

[9] M. Hatridge, S. Shankar, M. Mirrahimi, F. Schackert, K. Geerlings, T. Brecht, K. M. Sliwa, B. Abdo, L. Frunzio, S. M. Girvin, R. J. Schoelkopf, and M. H. Devoret, Science **339**, 178 (2013).

[10] K. W. Murch, S. J. Weber, C. Macklin, and I. Siddiqi, Nature (London) **502**, 211 (2013).

[11] N. Roch, M. E. Schwartz, F. Motzoi, C. Macklin, R. Vijay, A. W. Eddins, A. N. Korotkov, K. B. Whaley, M. Sarovar, and I. Siddiqi, Phys. Rev. Lett. **112**, 170501 (2014).

[12] P. Campagne-Ibarcq, L. Bretheau, E. Flurin, A. Auffèves, F. Mallet, and B. Huard, Phys. Rev. Lett. **112**, 180402 (2014).

[13] J. P. Groen, D. Ristè, L. Tornberg, J. Cramer, P. C. de Groot, T. Picot, G. Johansson, and L. DiCarlo, Phys. Rev. Lett. **111**, 090506 (2013).

[14] S. J. Weber, A. Chantasri, J. Dressel, A. N. Jordan, K. W. Murch, and I. Siddiqi, Nature (London) **511**, 570 (2014).

[15] D. Tan, S. J. Weber, I. Siddiqi, K. Mølmer, and K. W. Murch, Phys. Rev. Lett. **114**, 090403 (2015).

[16] Y. Yamamoto and H. A. Haus, Rev. Mod. Phys. **58**, 1001 (1986)

[17] R. Ruskov, A. N. Korotkov, and K. Mølmer, Phys. Rev. Lett. **105**, 100506 (2010).

[18] L. P. García-Pintos and J. Dressel, Phys. Rev. A **94**, 062119 (2016).

[19] S. Hacohen-Gourgy, L. S. Martin, E. Flurin, V. V. Ramasesh, K. B. Whaley, and I. Siddiqi, Nature (London) **538**, 491 (2016).

[20] J. Atalaya, S. Hacohen-Gourgy, L. S. Martin, I. Siddiqi, and A. N. Korotkov, npj Quantun Inf. **4**, 41 (2018).

[21] Y. Aharonov, D. Z. Albert, and L. Vaidman, Phys. Rev. Lett. **60**, 1351 (1988).

[22] H. M. Wiseman, Phys. Rev. A **65**, 032111 (2002).

[23] S. Gammelmark, B. Julsgaard, and K. Mølmer, Phys. Rev. Lett. **111**, 160401 (2013).

[24] Y. V. Nazarov and M. Kindermann, Eur. Phys. J. B **35**, 413 (2003).

[25] A. Franquet and Y. V. Nazarov, Phys. Rev. B **95**, 085427 (2017).

[26] Y. V. Nazarov and J. Danon, *Advanced Quantum Mechanics: A Practical Guide* (Cambridge University Press, Cambridge, 2013).

[27] H. M. Wiseman and G. J. Milburn, Phys. Rev. Lett **70**, 548 (1993).

[28] A. A. Clerk, M. H. Devoret, S. M. Girvin, F. Marquardt, and R. J. Schoelkopf, Rev. Mod. Phys. **82**, 1155 (2010).